HATSOPOULOS MICROFLUIDS LABORATORY
Department of Mechanical Engineering, Massachusetts Institute of Technology

How Dilute are Dilute Solutions in Extensional Flows?

Christian Clasen, J.P. Plog, W.-M. Kulicke, M. Owens, C. Macosko
L.E. Scriven, M. Verani, and Gareth H. McKinely

March 2006
HML Report Number 06-P-09

HML@MIT
http://web.mit.edu/fluids

How dilute are dilute solutions in extensional flows?

C. Clasen[*], J.P. Plog[*], W.-M.Kulicke[*], M. Owens[†§], C. Macosko[†], L.E. Scriven[†], M. Verani[‡], G.H. McKinley[‡]

[*] *Institute of Technical and Macromolecular Chemistry, University of Hamburg, Germany*
[†] *Department of Chemical Engineering and Material Science, University of Minnesota, Minnesota, USA*
[§] *current address: Drug Coating Process Developments, Boston Scientific, Maple Grove, MN., USA.*
[‡] *Hatsopoulos Microfluids Laboratory, Massachusetts Institute of Technology, Cambridge, MA., USA.*

Abstract

We investigate the concentration-dependence of the characteristic relaxation time of dilute polymer solutions in transient uniaxial elongational flow. A series of monodisperse polystyrene solutions of five different molecular weights ($1.8\times10^6 \leq M \leq 8.3\times10^6$ g/mol) with concentrations spanning five orders of magnitude were dissolved in two solvents of differing solvent quality (diethyl phthalate and oligomeric styrene). Optical measurements of the rate of filament thinning and the time to break-up in each fluid are used to determine the characteristic relaxation time. A lower sensitivity limit for the measurements was determined experimentally and confirmed by comparison to numerical calculations.

Above this sensitivity limit we show that the effective relaxation time of moderately dilute solutions ($0.01 \leq c/c^* \leq 1$) in transient extensional flow rises substantially above the fitted value of the relaxation time extracted from small amplitude oscillatory shear flow and above the Zimm relaxation time computed from kinetic theory and intrinsic viscosity measurements. This effective relaxation time exhibits a power-law scaling with the reduced concentration (c/c^*) and the magnitude of the exponent varies with the thermodynamic quality of the solvent. This scaling appears to be roughly consistent to that predicted when the

dynamics of the partially elongated and overlapping polymer chains are described within the framework of blob theories for semi-dilute solutions.

1 Introduction

The critical overlap concentration of polymer coils, denoted c^*, is one of the most important characteristic values of a polymer solution. It is generally accepted that at concentrations $c/c^* < O(1)$ the steric and frictional interactions of neighbouring polymer coils are negligible and the rheological response of the fluid is solely governed by the sum of the deformation and hydrodynamic interactions of the isolated polymer coils and solvent which comprise the polymer solution. When these conditions exist the theoretical description of a dilute solution given by the Rouse/Zimm theory is expected to be valid. At higher concentrations the solution becomes semi-dilute and eventually entangled depending on the degree of overlap of adjacent coils and their molar mass .

Graessley (Graessley 1980) provides a simple definition of c^* that is widely accepted for demarking the boundary separating the physical and rheological definition of dilute and semidilute polymer solutions:

$$c^* = \frac{0.77}{[\eta]} \tag{1}$$

where $[\eta]$ is the intrinsic viscosity of the polymer solution which depends on the molar mass of the chain according to the Mark-Houwink-Sakurada equation $[\eta] = K_{[\eta]} M^a$ where $K_{[\eta]}$ is a constant and the power-law index $0.5 \le a \le 0.8$ varies with the quality of the solvent.

However, the definition of diluteness in eq. (1) is only applicable for polymer coils that are not deformed greatly beyond their equilibrium configuration (for example in small amplitude oscillatory shear (SAOS) flow). In extensionally-dominated flow fields, at

conditions which satisfy the coil-stretch transition ($\dot{\varepsilon}\tau = 1/2$) a polymer coil becomes highly extended leading to an increased interaction volume within which the chains may overlap, as reported by Dunlap and Leal (Dunlap and Leal 1987). Consequently polymer-polymer interactions are possible even at concentrations $c/c^* < O(1)$. The improper use of a near-equilibrium definition to characterize dynamic changes in conformation and the associated rheological responses to deformation has lead to the recent introduction of the term "ultradilute" solution to describe polymer solutions that remain truly dilute even when the polymer chains are deformed well beyond their equilibrium state (Harrison *et al.* 1998).

Characterization of the rheological properties of dilute and ultradilute solutions has rarely been carried out in extensional flows, because the extensional rheometry of polymer solutions has proven to be an experimental challenge far more complex than performing rheological measurements in a steady or dynamic shear flow. The challenge in characterizing extensional flows is to create and not disturb a homogeneous flow field while employing a liquid whose rheological properties are simple enough that they can be compared with theory. Consequently, new methods for the quantitative study of dilute polymer solutions in extensional flows are desired. Recent developments in non-invasive experimental methods for characterizing extensional flow fields are reviewed in the monograph by Kausch & Nguyen (Nguyen and Kausch 1999).

The first mechanical studies of the state of stress for polymer solutions in a well-defined uniaxial flow field were made by Sridhar et al. (Matta and Tytus 1990; Sridhar *et al.* 1991) using the filament stretching device. A comparison of different approaches for realizing this type of experiment (Anna *et al.* 2001) showed for the first time the possibility of quantitative determination of the transient extensional viscosity for well-characterized dilute solutions in a purely uniaxial flow field. A recent overview of filament stretching rheometry is

given in (McKinley and Sridhar 2002). Filament stretching instruments are complex and expensive and, furthermore, reliable experiments are very difficult for low viscosity fluids with zero shear-rate viscosities less than ~0.5 Pa.s due to inertial and gravitational effects (McKinley and Sridhar 2002). Recent studies of jet break-up (Christanti and Walker 2001) and drop pinch-off (Amarouchene *et al.* 2001; Cooper-White *et al.* 2002) as well as the groundbreaking work of Entov and co-workers (Entov *et al.* 1988; Bazilevskii *et al.* 1990; Bazilevskii *et al.* 1997; Entov and Hinch 1997) have demonstrated the efficacy of capillarity-driven thinning flows for the determination of transient extensional material functions. Capillary-thinning devices have been developed recently by a number of laboratories (Liang and Mackley 1994; Kolte and Szabo 1999; McKinley and Tripathi 2000; Stelter and Brenn 2000; Anna and McKinley 2001; Bazilevskii *et al.* 2001; Stelter *et al.* 2002) and the dynamics of the elasto-capillary thinning process are reviewed in (McKinley 2005).

It is important to note the distinctions between the dynamics of capillary thinning and those of filament stretching rheometry for dilute polymer solutions. For example, Gupta et al. (Gupta *et al.* 2000) investigated the effects of varying the concentration and molar mass of dilute and semi-dilute polystyrene solutions on the extensional stress growth in filament stretching experiments. In order to ensure elastic stresses were large enough to be measured accurately and in order to overcome gravitational effects, they had to perform the tests at large extension rates $\dot{\varepsilon}$, corresponding to Weissenberg numbers $Wi = \tau_0 \dot{\varepsilon} >> 1$ where τ_0 is the longest relaxation time of the polymer solution. In this limit, the chain deformation becomes increasingly affine, and Brownian dynamics simulations and experiments both show that the measured curves of the transient extensional viscosity begin to superpose and approach a single limiting curve as a function of strain (Larson 2005). It is thus very difficult to probe directly the effects of concentration changes on the longest relaxation time of the solution. By contrast, the theoretical analysis by Entov and Hinch (Entov and Hinch 1997), in conjunction

with supporting experimental data (Anna and McKinley 2001), shows that the elasto-capillary balance achieved in capillary-thinning experiments results in a natural stretching rate of $\dot{\varepsilon} = 2/(3\tau_0)$ or, equivalently, a Weissenberg number $Wi = \tau_0\dot{\varepsilon} = 2/3$. This self-selected value is just sufficiently above the critical value of 0.5 (corresponding to the coil-stretch transition) to keep the polymer chain stretching such that the growing elastic stress balances the increasing level of capillary pressure in the thinning cylindrical thread. All of the shorter relaxation modes in the chain experience the same elongation rate $\dot{\varepsilon}$, corresponding to Weissenberg numbers below 0.5, and consequently their contributions to the material response decay. The dynamics of elasto-capillary thinning are therefore controlled directly by the longest relaxation process which corresponds to the unravelling of the entire chain. Capillary thinning and break-up experiments thus provide a convenient means for probing chain-chain interactions as a function of polymer concentration through measurements of the characteristic time-scale of the solution in a strong extensional flow.

Several investigations of transient elongational behaviour have been reported for a range of different polymers and molar masses (Liang and Mackley 1994; Bazilevskii *et al.* 1997; Stelter and Brenn 2000; Anna and McKinley 2001; Anna *et al.* 2001) in semi-dilute to dilute solutions. Recently Bazilevskii et al. (Bazilevskii *et al.* 2001), Stelter et al. (Stelter *et al.* 2002) and Tirtaatmadja et al. (Tirtaatmadja *et al.* 2006) have studied flexible polymers in dilute and ultradilute solution, finding that the characteristic relaxation time extracted from capillary-thinning or jet-thinning experiments continues to depend strongly on the concentration even below the critical concentration *c**, in contrast to expectations of the Rouse/Zimm theory . In addition, Bazilevskii et al. and Tirtaatmadja et al. observed a power-law dependency of the relaxation time on the concentration. Similar power-law variations of the rheological properties for apparently dilute aqueous polymer solutions have also been observed by Kalashnikov (Kalashnikov 1994) and by Tam and Tiu (Tam and Tiu 1993). We

also note that whereas Stelter *et al.*, Tirtaatmadja *et al.* and Christanti and Walker (Christanti and Walker 2001) all reported relaxation times that *exceeded* the expected relaxation time from Zimm theory, Bazilevskii et al. (Bazilevskii *et al.* 2001) also found that for very dilute solutions (down to concentrations as low as 0.2 ppm) the power-law scaling lead to relaxation times that fell *below* the predicted Zimm relaxation time.

In order to resolve this discrepancy, the present paper focuses on a detailed investigation of the capillary-thinning dynamics and break-up for dilute and ultra-dilute monodisperse polymer solutions. In order to quantitatively analyze the elasto-capillary thinning process and extract the longest relaxation time for very dilute solutions it is first necessary to reconsider carefully the fluid dynamics of filament thinning, in particular to answer the question of how much of the tensile stress in the thinning thread is carried by the polymer and how much by the solvent. In other words, we seek to understand under what physical conditions a coil-stretch transition that occurs on the molecular scale can affect the resulting macroscopic fluid dynamics. This provides an effective distinction between a dilute and an ultradilute polymer solution for this particular flow configuration.

In this paper we present experimental investigations of capillary thinning using high molar masses and nearly monodisperse polystyrene samples ($1.8 \leq M \leq 8.3 \times 10^6$ g/mol). The chains are dissolved in two different high and low viscosity solvents with qualities ranging from good (diethylphthalate) to near theta conditions (styrene oligomer) over a range of concentrations spanning five orders of magnitudes. We thus investigate the elongational response under semi-dilute, dilute and ultra-dilute conditions. In addition, numerical calculations (using a multimode FENE-P formulation) of the transient stress evolution in the thinning filament are utilized to determine the relative contribution of the polymer chains to the overall stress balance as a function of concentration and molar mass. This enables us to

determine the lower sensitivity limit of the capillary-thinning technique and to identify systematic discrepancies that can arise under very dilute conditions.

2 Experiment and Analysis Methods

2.1 Sample preparation

The polystyrene sample were provided by Polysciences Inc., Warrington, PA, USA (Sample A: M_w =1.8×10^6 g/mol, and Sample D: M_w =6.0×10^6 g/mol), Polymer Laboratories (PL), Amherst, MA, USA (Sample C: M_w =5.7×10^6 g/mol and Sample E: M_w =8.3×10^6 g/mol) and also Polymer Standard Services (PSS), Ontario, NY, USA (Sample B: M_w =2.8×10^6 g/mol). Molar mass M_w and polydispersity M_w/M_n were verified by size exclusion chromatography with a multi-angle light scattering detector. Two different batches of oligomeric styrene (Piccolastic A-5 Resin) as a solvent for Boger fluids were provided by Hercules, (Wilmington, DE, USA), the diethylphthalate (DEP) solvent was supplied by Merck, (Darmstadt, Germany) and used as received.

The solutions of polystyrene in styrene oligomer (Boger fluids) were prepared in two different ways:

a) Sample A (0.166 wt%), Sample B (0.025 wt%) and Sample D (0.107 wt%) were prepared by adding the polymer to the oligomer at room temperature and placing the samples in an oven at 100°C, without stirring (Sample A and D) and with repeated agitation (Sample B), until the polymer dissolved over several weeks.

b) Sample C (0.25 wt%) and Sample E (0.1 wt%) were prepared by dissolving the polymer in minute amounts of toluene, mixing with the oligomer and continuous evaporation

of the toluene at 10 Pa pressure under steady agitation of the sample at 50°C over several weeks, controlling the evaporation process by weight.

The different concentrations utilized in the experiments were achieved by diluting the above samples with the respective batch of Piccolastic A-5.

Preparation of the polystyrene/DEP solutions involved dissolving the respective amount of polymer in the solvent. Homogenization was achieved by slow continuous agitation over a period of time not shorter than 7 days.

The relevant physical data of the solutions are compiled in Table 1 and 2. The intrinsic viscosities $[\eta]$ of the polystyrene/diethylphthalate solutions were determined using a micro-Ubbelohde viscometer with a No. IIc capillary (Ø = 0.95mm) (Schott-Geräte GmbH, Mainz, Germany), the intrinsic viscosities for the polystyrene in styrene oligomer solutions (Boger fluids) were calculated from the respective Mark-Houwink-Sakurada equation. The finite extensibility parameter L was calculated from molecular parameters as described in Section 2.4. The solvent viscosities η_s of the Boger fluids were determined from fitting Eqs. (2) and (3) to small amplitude oscillatory shear (SAOS) data, the solvent viscosity η_s of the diethylphthalate was measured in steady shear via cone and plate. Surface tensions γ were experimentally determined utilizing a Krüss K10ST Tensiometer (Hamburg, Germany).

2.2 Shear rheology

The rheology of the test fluids in both steady and dynamic shear flow was investigated using an AR1000 N rheometer as well as two Rheometric Series ARES (TA Instruments, Newcastle, DE, USA) with cone and plate fixtures, Ø = 40 mm, cone angle = 0.04 rad.

The longest relaxation time τ_0 (as measured by shear flow experiments) was obtained by fitting the predictions of the Rouse/Zimm model for dilute solutions to the measured linear

viscoelastic moduli $G'(\omega)$ and $G''(\omega)$. For Boger fluids with an oligomeric solvent, an additional weak elastic contribution of the solvent to the total measured loss and storage modulus must be included:

$$G' = \frac{\eta_s \tau_s \omega}{1+(\tau_s \omega)^2} + \frac{cRT}{M_w} \sum_{i=1}^{N_{\text{modes}}} \left[\frac{(\tau_0 \omega)^2}{i^{4+2\tilde{\sigma}} + (\tau_0 \omega)^2} \right] \tag{2}$$

$$G'' = \frac{\eta_s \omega}{1+(\tau_s \omega)^2} + \frac{cRT}{M_w} \sum_{i=1}^{N_{\text{modes}}} \left[\frac{(\tau_0 \omega) i^{2+\tilde{\sigma}}}{i^{4+2\tilde{\sigma}} + (\tau_0 \omega)^2} \right] \tag{3}$$

where R = 8.314 J/mol K is the universal gas constant, ω is the angular frequency, T is the absolute temperature and τ_s is the relaxation time of the oligomeric solvent (Mackay and Boger 1987). The longest relaxation time τ_0 is connected to the Zimm spectrum τ_i with a number of modes N_{modes} by a recursion relationship:

$$\tau_i = \frac{\tau_0}{i^{2+\tilde{\sigma}}} \quad \text{for} \quad i = 1, 2, ..., N_{\text{modes}} \tag{4}$$

where $\tilde{\sigma}$ is a measure of the hydrodynamic interaction between the segments of the polymer chain and the surrounding solvent. This parameter can be related to the hydrodynamic interaction parameter h^* of the Zimm model via a correlation originally published by Thurston (Bird *et al.* 1987):

$$\tilde{\sigma} = -1.40 \left(h^* \right)^{0.78} \tag{5}$$

For negligible hydrodynamic interactions (h^* = 0) the Rouse spectrum is obtained, for dominant hydrodynamic interactions, as in the case of Boger fluids, the parameter h^* approaches a limiting value of 0.25, resulting in the Zimm scaling of $2+\tilde{\sigma} \approx 1.5$.

The number of modes can be varied depending on the desired resolution of the viscoelastic spectrum. The Hookean dumbbell corresponds to N_{modes} = 1. Amelar et al. (Amelar *et al.* 1991) suggest that the appropriate molecular mass associated with a single

spring should be in the range 5000 – 10000 g/mol for polystyrene, resulting in values for the samples in this report of N_{modes} = 240 - 1100. In practice due to the rapid decay of higher modes and the limited range of frequencies used, a smaller number of modes of $8 < N_{\text{modes}} < 15$ is sufficient for the determination of τ_0 and computation of the linear viscoelastic properties.

2.3 Capillary thinning experiments

The capillary thinning experiments reported here were carried out using (i) a CaBER version1 (Thermo Electron, Karlsruhe, Germany) using circular endplates with a diameter D_p = 6mm, and (ii) a self-built apparatus with endplates of diameter D_p = 3mm. In each case an approximately cylindrical liquid bridge of height h_0 was formed between the two endplates. Both setups employed a step strain to separate the plates from their initial distance h_0, reaching their final separation h_f in 50 ms. The mid-plane diameter evolution was followed using a laser micrometer (CaBER) or a Cohu CCD camera recording at 30 frames/second (self-built apparatus). The aspect ratio increases from an initial value $\Lambda_0 = h_0 / D_p$ to a final aspect ratio $\Lambda_f = h_f / D_p$. In the present experiments we use $\Lambda_0 = 0.5$ and $\Lambda_f = 1.3$ (CaBER) or $\Lambda_0 = 1.0$ and $\Lambda_f = 2.5$ (self-built apparatus) to minimize the pertubative effects of gravitational forces and fluid inertia (Slobozhanin and Perales 1993) and thus to keep the height h_0 of the fluid sample on the order of or below the capillary length l_{cap}

$$h_0 \le l_{cap} = \sqrt{\frac{\gamma}{\rho g}} \ . \tag{6}$$

with the surface tension γ and the fluid density ρ. For further details on the geometry and aspect ratios see Rodd et al. (Rodd *et al.* 2005).

2.4 Numerical calculations of elasto-capillary thinning

For numerical calculations of the transient evolution in the filament diameter $D(t)$ we follow the approach of Entov and Hinch (Entov and Hinch 1997). The governing stress balance in a thinning viscoelastic filament, consisting of the product of the solvent viscosity η_s times the extension rate $\dot{\varepsilon}$, the axial tensile forces F_z, the tensile stress difference arising from the dissolved polymer $\Delta\sigma_p$, the surface tension γ and gravitational forces (Eggers 1997), is given by:

$$3\eta_s\dot{\varepsilon} = \frac{4F_z(t)}{\pi D(t)^2} - \Delta\sigma_p - \frac{2\gamma}{D(t)} + \frac{\rho g D_0^2 h_0}{D(t)^2} \quad . \tag{7}$$

This expression can be simplified by noting that, once the gravitational forces are overcome by the symmetric axial flow induced by capillarity in the necked region, the last term on the right hand side can be neglected (Kolte and Szabo 1999; McKinley and Tripathi 2000). A quantitative comparison of the numerically calculated versus experimentally measured evolution of the mid-plane diameter $D(t)$ described in the following sections is therefore only suitable below a critical diameter of $D \lesssim 0.5 l_{cap}$. For our systems this constraint corresponds to filament diameters less than $D \lesssim 1\text{mm}$. The evolution of a self-thinning bridge is described by a self-similar solution and the evolution of the tensile force $F_z(t)$ can thus be related to the rate of change in the diameter $D(t)$. McKinley and Tripathi (McKinley and Tripathi 2000) showed that the coefficient of proportionality

$$X = \frac{F_z(t)}{\pi\gamma D(t)} \tag{8}$$

for the typical experimental conditions in a capillary thinning of a Newtonian liquid is given by X = 0.7127 as determined by Papageorgiu (Papageorgiou 1995) for self similar capillary pinch off of a viscous fluid. However, as the contribution of the elastic stresses becomes large

in comparison to the viscous stresses the filament becomes increasingly cylindrical and the correction factor X is predicted to approach unity (Entov and Hinch 1997)

Using Eq. (8), the force balance reduces to the following 'purely-local' or 'zero-dimensional' formulation incorporating the viscous stress of the solvent $3\eta_s\dot{\varepsilon}$, the capillary pressure $2\gamma/D$ and the additional tensile stress $\Delta\sigma_p$ from the polymer:

$$3\eta_s\dot{\varepsilon} = (2X-1)\frac{2\gamma}{D} - \Delta\sigma_p . \tag{9}$$

The polymer contribution $\Delta\sigma_p$ is taken here to correspond to a multimode FENE dumbbell model:

$$\Delta\sigma_p(t) = \sigma_{p,zz} - \sigma_{p,rr} = \sum_{i}^{N_{\text{modes}}} G_i f_i \left(A_{zz,i} - A_{rr,i}\right) . \tag{10}$$

The tensor **A** is the ensemble average second moment configuration tensor

$$\mathbf{A} = \sum_{\text{i=1}}^{N_{\text{modes}}} \mathbf{A}_i = \frac{\langle \mathbf{QQ} \rangle}{Q_{eq}^2/3} \tag{11}$$

of the entire chain normalized with the equilibrium coil size Q_{eq}^2. In the Rouse-Zimm theory the contribution G_i to the elastic modulus of each mode is invariant with mode number and is only a function of the number density of polymer chains in solution (Ferry 1980):

$$G = nk_BT = \frac{cRT}{M_w} \tag{12}$$

The evolution equations for the i^{th} mode of **A**, using a multimode FENE-P mode algorithm, are given by

$$\overset{\nabla}{\mathbf{A}}_i = -\frac{1}{\tau_i}\left(f_i\mathbf{A}_i - \mathbf{I}\right) \quad (\text{for } i = 1, 2, ..N_{\text{modes}}) \tag{13}$$

where $\overset{\nabla}{\mathbf{A}}_i$ is the upper convected derivative $\overset{\nabla}{\mathbf{A}}_i = \dot{\mathbf{A}}_i - \nabla\mathbf{v}^T \cdot \mathbf{A}_i - \mathbf{A}_i \cdot \nabla\mathbf{v}$ with $\dot{\mathbf{A}}_i$ denoting the substantial time derivative and $\nabla\mathbf{v}^T$ the velocity gradient tensor (Bird *et al.* 1987).

The finite extensibility factor f_i for each mode is connected to the finite extensibility parameter L^2 for the entire polymer chain by the expressions

$$f_i = \frac{1}{1 - \dfrac{tr\mathbf{A}_i}{L_i^2}} \tag{14}$$

$$L_i^2 = \frac{L^2}{i^{2\nu}} \tag{15}$$

The finite extensibility parameter L^2 for the entire chain can be fully described in terms of molecular parameters such as the C-C bond angle θ and the number of bonds j of a monomer unit with molar mass M_u, the characteristic ratio C_∞ for a given polymer and the excluded volume exponent ν:

$$L^2 = 3\left(\frac{j\left(\sin\theta/2\right)^2 M_w}{C_\infty M_u}\right)^{2(1-\nu)} \tag{16}$$

The axial and radial deformation components of the constitutive model of Eq. (13) satisfy the equations:

$$\dot{A}_{zz,i} - 2\dot{\varepsilon}A_{zz,i} = -\frac{1}{\tau_i}\left(f_i A_{zz,i} - 1\right) \tag{17}$$

$$\dot{A}_{rr,i} + \dot{\varepsilon}A_{rr,i} = -\frac{1}{\tau_i}\left(f_i A_{rr,i} - 1\right) \tag{18}$$

The time-varying deformation rate $\dot{\varepsilon}$ in a capillary thinning experiment can be expressed in terms of the rate of necking of the diameter D through the continuity equation by equating the local velocity gradients at the mid-plane in the axial and radial directions, leading to:

$$\dot{\varepsilon} = \frac{-2}{D}\dot{D} \tag{19}$$

This expression, when combined with the force balance from Eq. (9) and the definition of elastic stress in Eq. (10), defines the overall stress balance:

$$(2X-1)\frac{2\gamma}{D} = 3\eta_s\dot{\varepsilon} + \frac{cRT}{M_w}\sum_{i=1}^{N_{\text{modes}}} f_i\left(A_{zz,i} - A_{rr,i}\right) \tag{20}$$

Eqs. (17 - 20) form a coupled set of ordinary differential equations that can be solved numerically to describe the temporal evolution of the mid filament diameter in capillary thinning. Input parameters are given by the independently measured physical parameters of the polymer chain and the solution (molar mass M_w, finite extensibility L^2, surface tension γ, density ρ, solution viscosity η_0 and solvent viscosity η_s) and the initial state of the filament after cessation of the sudden extension (initial diameter D_0 and initial conformation $A^0_{zz,i}$).

We set $N_{\text{modes}} = 8$ for the following calculations. The (low) number of modes chosen here is justifiable by noting that during the period when elastic stresses dominate filament thinning the self-selected Weissenberg number for the flow is $We = \tau_0\dot{\varepsilon} = 2/3$, and is determined by the longest mode (Entov and Hinch 1997). All other modes N_i for $i > 1$ are in a relaxed state since their respective Weissenberg numbers (given by Eq. (4)) are below 0.5 until very near the end of the stretching process. These modes therefore do not contribute significantly to the total stress.

The unknown initial conformation and the initial stretch of the polymer after the step strain can be estimated according to the procedure proposed by Anna and McKinley (Anna and McKinley 2001). We assume that all three terms in Eq. (9) initially balance each other during the rearrangement of the fluid column at the cessation of the initial stretch. By replacing $\dot{\varepsilon} = 2/(3\tau_0)$ in the viscous contribution we obtain:

$$\frac{2\gamma}{D_0} - \frac{2\eta_s}{\tau_0} = \frac{cRT}{M_w} \sum_{i=1}^{N_{\text{modes}}} A_{zz,i}^0 \tag{21}$$

For the numerical calculations we assume an even distribution of the initial deformation over all modes; however, the numerical solutions were not sensitive to the choice of this initial deformation.

The parameter X in Eq. (8) and (20) is not constant over time. As the contribution of the elastic stresses becomes large in comparison to the viscous stresses the filament becomes increasingly cylindrical and the factor X should approach unity. A self-consistent determination of the axial force in the filament $F_Z(t)$ requires a full 1- or 2-dimensional numerical analysis of the thinning dynamics (Yao *et al.* 2000; Clasen *et al.* 2006) which is beyond the scope of the present study. The effect of varying X is rather small; however, for consistency in the numerical calculations, we retain the factor X for very low polymer concentrations in order to describe accurately the initial part of the Newtonian flow region. We adjust X and vary the value from 0.7127 for the pure solvent ($c \rightarrow 0$) to unity for polymer solutions which show a clear onset of polymeric effects in the necking process.

An example of the agreement between experimental measurements and the numerically calculated diameter evolution is shown in Fig. 1 for a dilution series of the Boger fluid from Sample E ($M_w = 8.3 \times 10^6$ g/mol), with the concentration spanning five orders of magnitude. Similar levels of agreement are obtained for each dilution series, and we now proceed to examine how to analyze experimental measurements of filament profiles.

2.5 Determination of relaxation times from elasto-capillary regime

Although we have just demonstrated above how it is possible to determine the longest relaxation time τ_0 by fitting the entire capillary thinning data, usually a simpler analysis is

employed. As noted by Entov and Hinch (Entov and Hinch 1997) for a viscoelastic polymer solution in which the chains become highly stretched, Eq. (9) offers the possibility of an *elasto-capillary* balance. The viscous stress of the solvent is negligibly small and the filament becomes a cylindrical thread ($X = 1$). Provided finite extensibility effects are not important ($L^2 \rightarrow \infty$), the decay rate in the measured diameter depends only on the longest relaxation time and is given by (Entov and Hinch 1997; Clasen *et al.* 2006):

$$\frac{D(t)}{D_0} = \left(\frac{GD_0}{4\gamma} \right)^{1/3} \exp\left(-t/3\tau_0\right) \tag{22}$$

The additional factor of $2^{-1/3}$ in the prefactor of Eq. (22), obtained from a complete 1-dimensional self similar analysis is missing in the original theory due to a simplifying approximation in the 0-dimensional theory (Clasen *et al.* 2006), though this does not change the exponential decay rate. The longest relaxation time τ_0 of the polymers undergoing molecular unravelling in the thinning filament can be easily obtained from this relationship by determining the slope of the linear regime in a semi-log plot as shown in Fig. 1 by the dashed lines. The validity of this approach and its consistency with other methods has been reported in several publications for a range of different polymers, molar masses and concentrations in dilute to semi-dilute solutions (Liang and Mackley 1994; Bazilevskii *et al.* 1997; Stelter and Brenn 2000; Anna and McKinley 2001; Anna *et al.* 2001; Bazilevskii *et al.* 2001; Stelter *et al.* 2002; Plog *et al.* 2005). In all of these cases, provided there is a *sufficiently large polymer concentration*, an elasto-capillary balance holds for a long enough period that the exponential decay of the filament can be observed and the data regressed to Eq. (22).

However, as we show in detail below, the more dilute a solution becomes, the harder it becomes to detect a distinct regime of purely exponential thinning. This is because the initial Newtonian flow and the finite extensibility of the polymer chains cannot be neglected during the short intermediate regime of exponential thinning. Nevertheless, linear fits of experimental

data on a semi log-plot to Eq. (22) are often performed even for very dilute solutions to extract a relaxation time and initially we will follow this procedure.

The numerical calculations described in §2.4 result in predicted profiles for the growth in the elastic stress and the decay rate of the filament diameter. The latter expression can be compared directly with the experimental observations. In cases for which the exponential decay of the filament could be observed over sufficiently long periods of time, the longest relaxation time τ_0 determined from reliable regressions of Eq. (22) to experimental data and the relaxation time used in numerical calculations coincide as can be seen for example in Fig. 1 for a concentration of 100 ppm. However, for very low polymer concentrations the numerically-predicted profile, calculated using the apparent relaxation time obtained from regressing the data in the very brief period of exponential thinning, does not match the experimentally observed evolution in the filament diameter. In these cases we use τ_0 as an *adjustable* parameter to fit the experiments with the numerical calculations and thus determine the governing relaxation time τ_0 for filament thinning. This discrepancy between an apparent longest relaxation time, determined from experimental data in the elasto-capillary thinning regime according to Eq. (22) (dashed line), and the longest relaxation time determined by fitting the numerical calculations can be observed in Fig. 1 for a concentration of 10 ppm. In the following Results & Discussion section we will compare τ_0 as determined by Eq. (22) to the value obtained by fitting with numerical calculations and provide a criterion for conditions under which Eq. (22) may be safely used.

3 Results and Discussion

3.1 Capillary thinning

We first present our experimental measurements of capillary thinning in viscous oligomeric solvents and in the low viscosity DEP solvent. Fig. 2 depicts the temporal evolution of the mid-plane diameter that can be determined experimentally. The figure shows three representative dilution series that demonstrate the critical characteristics of the thinning behaviour, the complete data set for all of the capillary thinning experiments can be found in Appendix A.

Fig. 2a shows the filament evolution of Boger fluids determined by analyzing still frames captured by a CCD camera. It is evident that the diameter resolution of this method is lower than that of the laser micrometer shown in Fig. 2b for Boger fluids and in Fig. 2c for diethylphthalate solutions. However, determination of the exponential decay of the diameter with time according to Eq. (22) is still possible using Fig. 2a because the onset of finite extensibility effects occurs below the resolution limit of the imaging system.

It can clearly be seen from Figs. 2a and 2b, that at early times the necking behaviour of all solutions follows the thinning behaviour of the Newtonian solvent as expected from the analysis of Entov and Hinch (Entov and Hinch 1997). The necking is controlled by a *visco-capillary* balance of the viscous stress $3\eta_s\dot{\varepsilon}$ in the force balance of Eq. (9) and the capillary pressure. In this regime the diameter varies linearly in time

$$D(t) = D_0 - \frac{(2X-1)\gamma}{3\eta_s}t \tag{23}$$

and the extension rate in the necking filament, given by

$$\dot{\varepsilon}(t) = \frac{2(2X-1)\gamma}{3\eta_s}\frac{1}{D(t)} \tag{24}$$

slowly climbs.

The polymeric stress associated with the initial conformation $A^0_{zz,i}$ (Eq. (21)) that is caused by the step strain, decays rapidly during the early stages of thinning since the extension rate is insufficient to keep even the longest mode excited. However, as thinning progresses the extension rate rises, the polymer coils become extended, and the system crosses over to a second phase of *elasto-capillary* thinning. In this regime the filament thins exponentially according to Eq. (22). It is clear from Fig. 2b that this crossover shifts to earlier times and higher values of $D(t)/D_0$ as the polymer concentration is raised. Finally, at late times, the finite extensibility limit of the unravelling polymer is approached and the FENE factor f_i (Eq. (14)) in the force balance for the filament can no longer be neglected and the thinning behavior deviates from the exponential regime of elasto-capillary thinning. In this third phase the decay rate becomes linear again corresponding to a viscous liquid with a very high and anisotropic elongational viscosity resulting from the fully extended polymer chains. The filament diameter evolves according to

$$D(t) = \frac{\gamma}{\eta_E}\left(t_{br} - t\right) \tag{25}$$

with t_{br} the break-up time and η_E the steady uniaxial elongational viscosity.

This third phase is not observed for the diethylphthalate solutions in Fig. 2c because the filament diameter drops below the resolution limit of the experiment before the effects of finite extensibility are observed. The initial phase of visco-capillary thinning in Fig. 2c also shows a strong concentration dependence at higher concentrations. This is because the viscous resistance to thinning is determined by the viscosity of the total entangled solution rather than by the pure solvent as is the case for dilute or semi-dilute Boger fluids shown in Fig. 2b.

The relaxation times τ_0 determined by fitting data from the intermediate elasto-capillary phase in Figs. 2 to Eq. (22) are shown in Fig. 3. The relaxation times show a strong dependence on the concentration and decrease monotonically with decreasing concentration. To understand the molar mass dependence, one has to keep in mind that the styrene oligomers used as solvents in this report had different viscosities (Table 1). Kinetic theory shows that the longest relaxation time of an isolated polymer coil in dilute solution is proportional to the solvent viscosity:

$$\tau_0 = \frac{1}{U_{\eta\tau}} \frac{\eta_p}{G} = \frac{1}{U_{\eta\tau}} \frac{[\eta]\eta_s M_w}{RT} \tag{26}$$

where $U_{\eta\tau} = \tau_\eta / \tau_0$ is the universal ratio of the characteristic relaxation time τ_η of a dilute polymer solution system and the longest relaxation time τ_0. The numerical value of the universal ratio depends on the relaxation spectrum of the specific constitutive model (Öttinger 1996). From Eq. (26) it can be seen that for a homologous series of polystyrene solutions the slightly *higher* relaxation times of the Boger fluid with $M_w = 5.7\times10^6$ g/mol in comparison to $M_w = 6.0\times10^6$ g/mol are explained by the higher solvent viscosity of the styrene oligomer used in this set of fluids (see Table 1).

In addition to the experimentally determined relaxation times, Fig. 3 depicts graphically (by broken lines) the expected variation in the critical concentration as calculated from the molar mass dependence of the intrinsic viscosity (Eq. (1)). These curves are obtained by extrapolating the observed trends of relaxation times to these respective concentrations. The intrinsic viscosity is typically measured using an Ubbelohde viscometer of appropriate bore size for the fluid of interest. The Mark-Houwink relation for polystyrene in DEP, which is a relatively good solvent at T = 25°C, was determined to be $[\eta] = 8.1\times10^{-3} M_w^{0.704}$ with M_w in the units of g/mol and $[\eta]$ in cm^3/g. However, it is not easy to determine the intrinsic

viscosity of the Boger fluids via a Huggins extrapolation of directly-measured shear viscosities because of the inherent imprecision of shear rheometry and the need to evaluate accurately the difference $\Delta\eta/(\eta_s c) = (\eta_0 - \eta_s)/(\eta_s c)$ as $c \to 0$. Although styrene oligomer should act as an athermal solvent and result in near-theta conditions (Anna *et al.* 2001), so far there have been no reliable reports of measured intrinsic viscosities for a pure polystyrene Boger fluid. Solomon and Muller (Solomon and Muller 1996) report intrinsic viscosity measurements of polystyrene dissolved in a mixture of the theta solvent dioctylphthalate and styrene oligomer. They obtained an excluded volume exponent ν of slightly less then the value of 0.5 expected for a theta-solvent. The poorer solvent quality may be explained by a preferential attraction of the better of the two solvents in the solvent mixture towards the high polymer, and the contraction of the coil to reduce its expansion into the poorer-quality solvent (Larson 2005). In the following we use the Mark-Houwink relation derived from Solomon and Muller and their exponent ν= 0.453 (corresponding to slightly poorer than theta conditions for our Boger fluids) in order to determine intrinsic viscosities from the molar mass for our calculations of the critical concentration from Eq. (1). However, the solvent quality of Boger fluids is still not fully understood, and it should be born in mind that the calculated Zimm times in the following are imprecise due to this uncertainty in the intrinsic viscosities.

To circumvent this difficulty in the definition of the critical concentration, in addition to Eq. (1) we have also included in Fig. 3 a purely geometrical calculation for the coil overlap conditions in Boger fluids, derived from the mean square size of a polymer coil in its random walk configuration (Graessley 1980; Kulicke and Clasen 2004):

$$c^*_{R_G} = \frac{M_w}{\frac{4}{3}\pi \left\langle R_G^2 \right\rangle^{\frac{3}{2}} N_A} \tag{27}$$

The radius of gyration R_G, assuming near-theta conditions for the Boger fluids, can be calculated from molecular parameters including the C—C bond length b, the monomer molar mass M_u, and the characteristic ratio C_∞ for a given polymer (Kulicke and Clasen 2004):

$$R_g = \sqrt{\frac{b^2 C_\infty M_w}{3M_u}} \tag{28}$$

For polystyrene b = 0.154 nm, C_∞ = 9.6 and M_u = 104 g/mol. The critical concentrations for the solutions of polystyrene/styrene oligomer and polystyrene/DEP studied in the present work are listed in Tables 3 and 4.

The measured relaxation times for the PS/DEP solutions in Fig. 3 span the range from close-to, or above, the critical concentration into the semi-dilute regime, whereas the measured relaxation times of the Boger fluids lie in a regime below even the most conservative definition of c^*. In these dilute solutions the relaxation times of isolated coils should be *independent* of the concentration according to Eq. (26). In contrast to this expectation, the experimental relaxation times show a strong and monotonic decrease as the concentration is reduced to well below the critical concentration. Similar observations of concentration dependent relaxation times in capillary thinning experiments below c^* have recently been reported by Bazilevskii et al. (Bazilevskii *et al.* 2001) and Stelter et al. (Stelter *et al.* 2002) for polyacrylamide in water/glycerol mixtures and by Tirtaatmadja et al. (Tirtaatmadja *et al.* 2006) for polyethylene oxide in water/glycerol mixtures.

3.2 Small amplitude oscillatory shear

Capillary thinning experiments yield the characteristic unravelling time associated with strong flows and large molecular deformations. These values may also be compared to the relaxation times measured for each fluid in weak flows and small deformation conditions. Lindner et al. (Lindner *et al.* 2003) calculated relaxation times for dilute aqueous solutions as

low as 250 ppm from normal stress data fitted to an appropriate constitutive equation, and found good agreement with the expected Zimm relaxation times. However, for the Boger fluids investigated in this report the elastic response can be directly observed to even lower concentrations using small amplitude oscillatory shear (SAOS) flow (Anna *et al.* 2001). The Zimm relaxation times for the polystyrene Boger fluids have been obtained from regressing the expressions for the linear viscoelastic moduli G' and G'' (Eq. (2) and (3)) to the measured experimental data. A representative example of the resulting fits to the oscillatory shear data is presented in Fig. 4a. At low frequencies the elastic modulus is dominated by the Zimm spectrum of the high molar mass polystyrene solute, allowing for unambiguous determination of the longest relaxation time τ_0, while at high frequencies the response is dominated by the weak elasticity of the oligomeric solvent.

However, with progressively decreasing concentration, the elastic modulus $G = cRT/M_w$ of the solute decreases and the contribution of the high molar mass polystyrene to the measured elastic moduli is increasingly obscured by the oligomer. This can be seen in the data presented in Fig 4b for a dilution series of a single molar mass of polystyrene. Consequently, accurate fitting of the Zimm spectrum is hindered at low concentrations and the extraction of an accurate longest relaxation time τ_0 becomes less robust.

For low frequencies, $\tau_s\omega \ll 1$, the first term in Eq. (2) can be neglected and the expression reduces to the pure Zimm spectrum. The longest relaxation times obtained from the fits for each fluid can then be used to verify the expected scaling of the reduced storage modulus $G'M_w/c$ with the reduced frequency $\tau_0\omega$.

$$\frac{G'M_w}{c} \sim \sum_{i=1}^{N_{\text{modes}}} \left[\frac{(\tau_0\omega)^2}{i^{4+2\tilde{\sigma}} + (\tau_0\omega)^2} \right] \tag{29}$$

Fig. 4c shows the reduced moduli for the fluids used in the present study that exhibited sufficient elastic response from the polystyrene solute to perform satisfactory fits to Eq. (2). The underlying Zimm spectrum can clearly be observed in Fig. 4c from the common mastercurve at low reduced frequencies $(\tau_0\omega) \ll 1$.

The longest relaxation times obtained from this analysis are represented in Fig. 5 as dimensionless values τ_0 / τ_Z plotted as a function of c/c^* (with c^* being the critical concentration from Eq. (1)). To obtain the Zimm relaxation time τ_z (assuming a Zimm spectrum for the isolated polymer coil in a solvent), the universal ratio in Eq. (26) can easily be calculated from Eq. (4) to give

$$U_{\eta\tau} = \frac{\sum_i \tau_i}{\tau_0} \cong \sum_i \frac{1}{i^{2+\tilde{\sigma}}} \tag{30}$$

where $\tilde{\sigma}$ is given by the Thurston relation, Eq. (5), giving a Zimm relaxation time τ_Z of:

$$\tau_z = \frac{1}{\sum_i \frac{1}{i^{2+\tilde{\sigma}}}} \frac{[\eta]\eta_s M_w}{RT} \tag{31}$$

The resulting values of τ_Z for each fluid are given in Table 1 and 2. It is clear from Fig. 5 that at low concentrations the Zimm relaxation time is recovered accurately from SAOS experiments. Approaching the critical concentration, the relaxation time slowly increases due to the growing importance of intermolecular interactions with increasing concentration. The form of the mastercurve in Fig. 5 can be rationalized by noting that the polymeric contribution to the viscosity η_p in Eq. (26) can be expanded in the concentration as for example by the Martin equation (Kulicke and Clasen 2004):

$$\eta_p = \eta_s c[\eta] e^{K_M c[\eta]} \tag{32}$$

where K_M is the Martin coefficient. In combination with Eqs. (1), (12), (26), (30) and (31) this gives a dependence of the longest relaxation with the reduced concentration c/c^* of the form:

$$\tau_0 = \frac{1}{U_{\eta\tau}} \frac{[\eta]\eta_s M_w}{RT} \exp\left(K_M 0.77 \frac{c}{c^*} \right) = \tau_z \exp\left(K_M 0.77 \frac{c}{c^*} \right) \tag{33}$$

Using this approach, one can also plot the longest relaxation times obtained from the capillary thinning experiments in their reduced form τ_0 / τ_Z as a function of c/c^* as shown in Fig. 6. The superposition of data for different molar masses shows the expected scaling of the longest relaxation time $\tau_0 \sim M_w^{3\nu}$ obtained from the definition of the Zimm relaxation time in Eq. (31) with molar mass and solvent quality.

However, comparing this mastercurve to the relaxation times determined from the SAOS experiments of Fig. 5, (depicted as a broken line in Figure 6), two important distinctions are noted. Firstly, the relaxation times in uniaxial extension deviate at much lower concentrations from the asymptotic value given by Zimm theory in comparison to the small amplitude oscillatory shear experiments. In addition, the data in Fig. 5 indicates that at very low concentrations the relaxation time determined from capillary thinning appears to fall *below* the Zimm relaxation time. This puzzling observation is in agreement with observations made by Bazilevskii et al. (Bazilevskii *et al.* 2001) for very dilute polyacrylamide/ water/glycerol solutions. For an explanation of this peculiar phenomenon, one needs to examine in greater detail the thinning dynamics at very low concentrations as we show below.

3.3 Transient stress evolution

In general, lowering the concentration of a polymer in solution so that the relaxation time approaches its limiting Zimm relaxation time leads to the question of whether the flow in the thinning filament is still dominated by the timescale of the polymer or by that of the visco-capillary flow in the Newtonian solvent. A discussion of these time scales is given by

(McKinley 2005). For viscous Newtonian fluids the relevant timescale is the viscous capillary break-up time $t_{visc} = \eta_0 D_0 / (2\gamma)$. The ratio of this time scale to the longest relaxation time τ_0 in the polymer defines the elastocapillary number:

$$Ec = \frac{\tau_0}{t_{visc}} = \frac{2\tau_0 \gamma}{\eta_0 D_0} \tag{34}$$

For elastocapillary numbers below unity, the elastic stresses from the polymeric contribution to the observed flow are negligible compared to the viscous stresses and a capillary thinning experiment will not allow the extraction of a polymeric relaxation time. For dilute solutions, the polymeric contribution to the elasto-capillary number is principally through the molar mass dependence of the relaxation time. We therefore expect a lower limit in the molar mass for a given experimental setup with specified values of the surface tension γ, solvent viscosity η_0 and initial radius.

However, even for $Ec > 1$, observation of a filament thinning process dominated by the elasticity (as indicated by a corresponding exponential decrease of the filament diameter according to Eq. (22)) may not be possible if the concentration is not high enough. The transition from the initial balance of capillary and viscous stresses to the balance of capillary and elastic forces is progressively shifted to later times, as the polymer concentration c and the elastic modulus G are progressively reduced (see Eqs. (12) and (20)). Physically, it is clear that if the polymer concentration is too small the elastic stress term on the right hand side of Eq. (20) cannot balance the squeezing action arising from capillary pressure. Instead viscous stresses from the oligomeric solvent provide the dominant resistance to thinning. Because the elastic stresses evolve nonlinearly (exponentially) with time, it is not straightforward to determine the crossover conditions from a simple order of magnitude scaling estimate and instead we turn to numerical calculations.

In the left hand column of Figs. 7 a-c we show the temporal variation in the different contributions to the overall stress, obtained from the numerical integration of Eqs. (17) - (20), for three different concentrations of the same polymer. The capillary pressure, which drives the flow, increases monotonically in time and ultimately diverges at a critical timescale interpreted as the break-up time, t_{br}. The dashed and dotted lines show the relative contributions of the viscous and elastic stresses respectively. As the concentration is lowered, the transition from a solvent-dominated to an elasticity-dominated flow shifts to later times during the thinning process. While this shifts the elastocapillary regime to smaller radii and therefore towards the lower resolution limit of the experimental setup, it also means a faster approach to the finite extensibility limit of the polymer.

In the right hand column of Figs. 7 a-c we show the individual modal contributions to the polymer stretch tensor **A** as a function of time scaled by the longest relaxation time. For the bulk of the capillary thinning process, the majority of the stress is carried by the longest mode (i = 1). Exponential decay in the radius corresponds directly to exponential growth in the principal stretch difference $A_{zz,1}$-$A_{rr,1}$ of the longest mode. As the deformation rate diverges close to the singular break-up event, the shorter modes begin to stretch rapidly and ultimately all modes approach their relevant finite extensibility limit. Once the higher modes of the configuration **A** reach their finite extensibility limit, the flow pattern again crosses over to a Newtonian-like flow behaviour. Extraction of a relaxation time by a simple exponential fit to Eq. (22) is therefore not possible once finite extensibility effects start to dominate the flow. At low concentrations, the combined effects of finite extensibility and a low initial concentration or modulus eliminate the possibility of a clear elasto-capillary balance at the micro-scale or a macroscopic detection of an exponential decay regime in this rheometric device, even though there is a well-defined underlying microscopic relaxation time for the fluid itself. This is also demonstrated in Fig. 8 by a series of numerical calculations for a

progressively diluted polystyrene Boger fluid. The longest relaxation time τ_0 for these calculations is chosen to be constant for all dilutions and the value is assumed to agree with the Zimm time τ_z. As one can see, the break-up times progressively decrease with decreasing concentration. At a concentration of c = 100 ppm ($c/c^* = 0.012$) there is a clear region of elasto-capillary decay and a filament decay rate that would agree with the expected rate $1/(3\tau_0)$. However, the slopes of the curves in the intermediate thinning regime appear to become steeper in the semi-log plot of Fig. 8 and this suggests apparent relaxation times that are *below* the Zimm time used for these calculations. This effect is further amplified by a gradual "smearing out" of the transition from the initial Newtonian thinning to the elasto-capillary regime.

3.4 The critical concentration c[§]

It is clear from the above model calculations that capillary thinning instruments have a minimum detectable elasticity limit, in much the same way that conventional torsional rheometers used in SAOS tests have a minimum value of elastic modulus that can be reliably detected. The ultimate limit of the capillary thinning experiment for the observation of the polymeric contribution can be seen in Fig. 7c. Even though all modes of the polymer stretch have reached their finite extensibility limit at late times, the contribution of the viscous stresses from the solvent still dominates the flow behaviour. The minimum concentration at which the total elastic stress of the fully expanded coils just balances the viscous stresses of the solvent can be estimated from the force balance in Eq. (9).

Following Entov and Hinch (Entov and Hinch 1997), close to the finite extensibility limit we expect $A_{zz} >> A_{rr}$ and a negligible temporal change of the polymer stretch A_{zz}, the relevant evolution equation (Eq. (17)) then reduces to

$$2\dot{\varepsilon}A_{zz,i} = \frac{1}{\tau_i} f_i A_{zz,i} \,. \tag{35}$$

This gives for the finite extensibility factor f_i:

$$f_i = 2\dot{\varepsilon}\tau_i \tag{36}$$

and with tr$\mathbf{A} \approx A_{zz}$ a solution for A_{zz} at the finite extensibility limit:

$$A_{zz,i} = L_i^2 \left(1 - \frac{1}{2\dot{\varepsilon}\tau_i}\right) \tag{37}$$

Substituting Eqs. (36) and (37) into the equation for the polymeric contribution to the stress $\Delta\sigma_p$ (Eq. (10)) with $A_{zz} >> A_{rr}$ we obtain for the finite extensibility limit:

$$\Delta\sigma_p = \sum_i^{N_m} 2G\dot{\varepsilon}\tau_i L_i^2 \left(1 - \frac{1}{2\dot{\varepsilon}\tau_i}\right). \tag{38}$$

As the filament radius approaches zero, the stretch rate diverges and the final term becomes negligible. Also neglecting the marginal contribution of the higher modes of the spectra for relaxation time τ_i (Eq.(4)) and finite extensibility L^2_i (Eq. (15)) we finally obtain the following expression for the polymer stress once the longest mode has reached its finite extensibility limit:

$$\Delta\sigma_p \approx 2G\dot{\varepsilon}\tau_z L^2 \tag{39}$$

From this we obtain a constant polymer extensional viscosity $\eta_E \approx 2G\tau_z L^2$ for the finite extension limit. The viscous stress carried by the solvent will dominate at late times if the term $3\eta_s\dot{\varepsilon}$ in Eq. (9) becomes larger than the polymer stress $\Delta\sigma_p$ given by Eq. (39). The polymer contribution to the total stress is thus only observable in capillary thinning experiments if

$$\frac{2G\tau_z L^2}{3\eta_s} > 1. \qquad (40)$$

Substituting the modulus from Eq. (12), we derive an expression for the lowest possible polymer concentration for an observable elastic contribution to a capillary break-up experiment. We denote this concentration $c^{\S}$ and require

$$c > c^{\S} = \frac{3}{2}\frac{M_w \eta_s}{RT\tau_z L^2} \qquad (41)$$

or by combining this expression with the Zimm relaxation time given by Eq. (31):

$$c > c^{\S} = \frac{3}{2}\frac{U_{\eta\tau}}{[\eta] L^2} \qquad (42)$$

At this critical concentration $c^{\S}$ the extended polymer is still contributing partially to the overall stress at late times, however, this concentration marks the point below which the polymer will carry less stress than the solvent even if it is fully extended.

The critical concentrations $c^{\S}$ for the polystyrene solutions can easily be calculated from molecular parameters and are shown in Table 3. The value of $c^{\S}$ was also chosen for the numerical calculation in Fig. 7c and it can clearly be seen that at $c = c^{\S}$ the viscous and polymeric stresses provide the same contribution to the overall stress balance at late times. The critical concentration $c^{\S}$ is also indicated in Figs. 2b) and 14b) in addition to the experimental thinning data. This theoretical estimate for the critical concentration describes quite well the borderline between purely viscous thinning behaviour and the onset of significant elasto-capillary effects for all three molar masses.

3.5 Relaxation times from numerical calculations

Given these limitations to directly extracting the relaxation time from elasto-capillary thinning, we have also used a different approach to obtain good estimates of the relaxation

times close to the critical concentration limit $c^{\S}$ given by Eq. (41). Numerical integrations of Eqs. (17) - (20) for the filament thinning process with the longest relaxation time τ_0 as the only adjustable parameter are used to obtain the best agreement with the experimentally-measured filament thinning profiles first presented in Fig. 2. Samples of the resulting best fits to the experimental data are shown for several decades of concentration and two different molar masses in Figs. 9 and 10. It is clear that excellent agreement with the measured diameter data can be achieved by adjusting the value of $\tau_0(c)$, even though the profiles of the stress evolution are not elastically-dominated at low concentrations.

The relaxation times derived from these numerical calculations in Figs 9 & 10 can also be used to regenerate the reduced data or master curve originally presented in Fig. 6. These new results are presented in Fig. 11 and it is clear that the true relaxation time in uniaxial extension asymptotically approaches a constant value at low concentrations in accordance with the concentration-independent relaxation times directly measured with the SAOS experiments at low concentrations. However, one must note that the constant value of the reduced relaxation times obtained from our numerical calculations for molecular unravelling in uniaxial extension is slightly lower than unity: the average molecular unravelling time from Fig. 11 at low concentrations is a factor of ~ 1.4 lower than the corresponding Zimm relaxation times. This differential is probably a consequence of describing the unravelling chain as a suspension of uncoupled dumbbells. We do this for computational simplicity only; a more realistic description would treat the chain as a fully coupled set of discrete relaxation modes or through Brownian dynamics simulations (Doyle *et al.* 1997; Ghosh *et al.* 2001).

3.6 Enhanced relaxation times in extensional flow

The relaxation times obtained from the numerical calculations of transient uniaxial flow at higher concentrations are, as expected, in very good agreement with the relaxation times directly extracted from the fit of Eq. (22) to the experimental data. Still, these values are substantially higher than the relaxation times obtained from the oscillatory shear flow experiments.

This can also be observed in the data presented in Fig. 12 for solutions of polystyrene in the good solvent diethylphthalate. Since the DEP solutions have a much smaller viscosity than the Boger fluids, the observable range of relaxation times is shifted to higher concentrations, as determined by the low viscosity limit of the elastocapillary number in Eq. (34). For these solutions it is not possible to obtain relaxation times close to the Zimm limit by capillary thinning or via SAOS experiments. However, we are able to determine the numerical value of the constant in the structure-property relationship of Eq. (32) to be $K_M = 0.35$ by regression to the experimental viscometric data as shown in Fig. 13. For these DEP solutions, the intrinsic viscosities can be directly determined and used in the subsequent calculation of c^*. The corresponding prediction for the concentration-dependence of the longest relaxation time (as given by Eq. (33)) is also shown in Fig. 12 by the solid line. Again, it can be seen that the relaxation times determined from capillary thinning start to rise above the dilute limit at much smaller concentrations than theoretically expected from Eq. (33).

The onset point for the increase in the characteristic relaxation times for elongational flow gives a rough estimate of a critical concentration for ultradilution. Below this concentration (but still above the experimental sensitivity limit $c^{\S}$) we are able to observe the presence of the polymer in terms of a delayed break-up time and a deviation from the thinning behaviour of the viscous Newtonian solvent. The relaxation time or, more descriptively, the molecular unravelling time is, in this case, constant and corresponds to that of the single

polymer coil. With further decreases in the solute concentration the transition to an elasto-capillary balance shifts to progressively later times and smaller filament diameters. It thus becomes increasingly hard to resolve, given the optical constraints of the experimental instrumentation.

Above the ultradilution point the concentration of the polymer coils is high enough that the long-range interactions between unravelling polymer coils leads to an increase in the effective relaxation time of the solution. The scaling of the relaxation time with the reduced concentration in this regime appears to obey the following relation proposed by Tirtaatmadja et al. (Tirtaatmadja *et al.* 2006):

$$\frac{\tau_0}{\tau_Z} \sim \left(\frac{c}{c^*} \right)^m \tag{43}$$

We determined an exponent of $m = 0.58$ in Fig. 12 for polystyrene in the relatively good solvent DEP in comparison to $m = 0.65$ observed by Tirtaatmadja et al. (Tirtaatmadja *et al.* 2006) for PEO in glycerol/water mixtures. In contrast to this, for the polystyrene dissolved in the near theta solvent of styrene oligomer we obtain an exponent $m = 0.89$ from Fig. 11.

One possible explanation for the dependence of the power-law exponent m on the solvent quality can be obtained from scaling theory for unentangled semi-dilute solutions. In weak flows and for small molecular deformations close to equilibrium, such scaling theories are expected to hold only for concentrations above the overlap concentration c^*. However, for strong flows, such as those encountered in the present case of capillary thinning, the pervaded volume occupied by each expanding polymer coil increases rapidly due to unravelling. It is thus perhaps reasonable to imagine that we approach a semi-dilute state of polymer interaction in which neighboring chains overlap and interact. In such a regime, the scaling assumptions appropriate for semi-dilute 'blob' theories should hold (Rubinstein and Colby 2003). This

gives rise to a correlation length $\xi \approx bg^{\nu}$ where b is the monomer length and g is the number of monomers within the blob. On length scales shorter than the correlation length intra-chain hydrodynamic interactions dominate; however they are screened out on larger scales. Once the elongating polymer chains have expanded to become space-filling, the concentration in an individual correlation blob should be equal to the overall solution concentration $c \sim gb^3/\xi^3$ and the correlation length is thus

$$\xi \sim bc^{-\frac{\nu}{3\nu-1}} \tag{44}$$

The correlation length thus decreases with increasing concentration. Inside a correlation blob, single chain hydrodynamics dominate and therefore a Zimm relaxation time of the form given in Eq. (26) applies. The longest relaxation time τ_ξ of a blob is proportional to the correlation volume ξ^3 (Rubinstein & Colby, 2003) and therefore:

$$\tau_\xi \approx \frac{\eta_s}{k_B T}\xi^3 \sim \frac{\eta_s b^3}{k_B T}c^{-\frac{3\nu}{3\nu-1}} \tag{45}$$

On length scales larger than ξ, the internal hydrodynamic interactions are screened out. We thus expect Rouse dynamics to dominate the chain-chain interactions of the expanded and overlapping coils. The relaxation time of the whole chain, consisting of $M_w/(M_u g)$ blobs, each with a relaxation time τ_ξ, thus has the following concentration dependence:

$$\tau_0 \approx \tau_\xi\left(\frac{M_w}{gM_u}\right)^2 \sim \frac{\eta_s b^3}{k_B T}\left(\frac{M_w}{M_u}\right)^2 c^{\left(\frac{2-3\nu}{3\nu-1}\right)} \tag{46}$$

Finally, the coil overlap concentration can be substituted into Eq. (46) by noting that $c^* \sim M_w^{1-3\nu}$ to obtain

$$\frac{\tau_0}{\tau_Z} \sim \left(\frac{c}{c^*}\right)^{\left(\frac{2-3\nu}{3\nu-1}\right)} \tag{47}$$

Comparing the exponent m from Eq. (43) with the exponent $m_{\text{theory}} = (2-3\nu)/(3\nu-1)$ from Eq. (47) we are able to capture at least the general trend of observed slopes with the solvent quality as shown in Table 5.

Stoltz et al. (Stoltz *et al.* 2006) have recently investigated finite concentration effects in planar elongational flow using Brownian dynamics simulations. They also find that hydrodynamic interactions and excluded volume effects lead to a marked concentration-dependence of the extensional rheological properties of supposedly-dilute polymer solutions at concentrations as low as $0.1c^*$. Our data shown in Figs 11 & 12 appears to be in good agreement with such findings.

4 Conclusions

In the experiments and calculations reported here, the relaxation times of a series of model dilute and semi-dilute polystyrene solutions have been determined over a wide range of concentrations and molecular weights in both shear flow and uniaxial extensional flow.

It should be noted that the experiments with very dilute solutions presented in this paper have been performed principally using very viscous solvents. The lack of data for very dilute (and therefore low viscosity) solutions of PS in DEP is a consequence of the Ohnesorge number $Oh = \eta_0/\sqrt{\rho\gamma R_0}$ being much less than unity. It is thus a balance of *inertia* and elasticity that controls the filament thinning-process in such solutions (McKinley, 2005), resulting in rapid rupture during the stretching phase or the formation of bead-on-string

structures in capillary thinning experiments. These experimental difficulties associated with low viscosity fluids are discussed in more detail by Rodd *et al.* (Rodd *et al.* 2005).

The linear viscoelastic properties of the dilute polystyrene solutions studied in this work are accurately described by the Zimm model, and the variation of the viscometric properties in the semi-dilute regime can be described by correlations such as the Martin equation. Capillary thinning measurements employing two different instruments show that in transient uniaxial extensional flow the effective relaxation time – or more accurately the molecular unravelling time – is a strong function of the polymer concentration, even at concentrations well below the conventional coil overlap concentration c^*. Interpretation of this finding must be approached with care because capillary thinning devices have a minimum sensitivity limit, just as any other rheometric device. A force balance shows that there is a critical concentration, denoted $c^{\S}$, below which polymeric stresses are insufficient to support the elasto-capillary balance that is required for successful and unambiguous determination of the relaxation time.

Numerical calculations show that for concentrations close to $c^{\S}$ the finite extensibility of the polymer chains and viscous stresses from the solvent lead to a systematic bias and under-prediction of the true relaxation time of the polymer solution being tested. The widely-used 'elasto-capillary balance' – which defines how the experimentally-determined relaxation time of the solution is extracted – cannot be sustained below this critical concentration limit due to the magnitude of the underlying solvent stress and the finite extensibility of the chains. Consequently a spurious concentration-dependence of the macroscopically-measured relaxation time is obtained, even though the microscopic properties of the solution are unchanged.

Provided that the limit $c < c^{\S}$ is avoided, capillary thinning measurements – in conjunction with numerical calculations – show that the fitted relaxation times are in good agreement with both the Zimm relaxation times determined from molecular theory and those obtained from small amplitude oscillatory shear measurements of the linear viscoelastic moduli. However, as the concentration is slowly increased over the range $c^{\S} \leq c \leq c^*$, the value of the molecular unraveling time characterizing transient elongation increases substantially above the relaxation time that is predicted theoretically or measured under near-equilibrium conditions. Recent Brownian dynamics simulations incorporating excluded volume effects and inter-chain hydrodynamic interactions in planar elongational flows also show similar finite concentration effects for $0.1c^* \leq c \leq c^*$ (Stoltz *et al.* 2006).

When the characteristic time constant determined experimentally for a wide range of molecular weights is normalized with the Zimm time constant, the result is found to increase according to a power-law in the reduced concentration c/c^*, with an exponent that varies with the thermodynamic quality of the solvent. This power-law scaling with the reduced concentration appears to be approximately consistent with treating the dynamics of unravelling and overlapping polymer chains within the framework of 'blob' scaling theories for semi-dilute solutions.

Acknowledgments

The portion of this research carried out at MIT was supported by the NASA Microgravity Fluid Dynamics program (Code UG) under grant NCC3-610. Mike Owens acknowledges financial support from the Industrial Partnership for Research in Interfacial and Materials Engineering (IPRIME) at the University of Minnesota. Jan Plog was supported by a

research grant from the Young Scientists Fellowship of Hamburg University (Promotionsstipendium der Hamburgischen Nachwuchsförderung).

References

Amarouchene, Y., D. Bonn, J. Meunier and H. Kellay, "Inhibition of the finite-time singularity during droplet fission of a polymeric fluid". Physical Review Letters **86**, 3558-3561 (2001).

Amelar, S., C. E. Eastman, T. P. Lodge and E. D. Vonmeerwall, "How Good Is the Bead-Spring Model". Journal of Non-Crystalline Solids **131**, 551-555 (1991).

Anna, S. L. and G. H. McKinley, "Elasto-capillary thinning and breakup of model elastic liquids". Journal of Rheology **45**, 115-138 (2001).

Anna, S. L., G. H. McKinley, D. A. Nguyen, T. Sridhar, S. J. Muller, J. Huang and D. F. James, "An interlaboratory comparison of measurements from filament- stretching rheometers using common test fluids". Journal of Rheology **45**, 83-114 (2001).

Bazilevskii, A. V., V. M. Entov, M. M. Lerner and A. N. Rozhkov, "Degradation of polymer solution filaments". Vysokomolekulyarnye Soedineniya Seriya A & Seriya B **39**, 474-482 (1997).

Bazilevskii, A. V., V. M. Entov and A. N. Rozhkov, "Liquid filament microrheometer and some of its applications", at *Third European Rheology Conference.* (1990).

Bazilevskii, A. V., V. M. Entov and A. N. Rozhkov, "Breakup of an Oldroyd liquid bridge as a method for testing the rheological properties of polymer solutions". Vysokomolekulyarnye Soedineniya Seriya A **43**, 716-726 (2001).

Bird, R.B., O. Hassager, R.C. Armstrong and C.F. Curtiss, *Dynamics of polymeric liquids - Kinetic theory,* Vol. 2. John Wiley & Sons, New York (1987).

Christanti, Y. and L. M. Walker, "Surface tension driven jet break up of strain-hardening polymer solutions". Journal of Non-Newtonian Fluid Mechanics **100**, 9-26 (2001).

Clasen, C., J. Eggers, M. A. Fontelos, J. Li and G. H. McKinley, "The beads-on-string structure of viscoelastic threads". Journal of Fluid Mechanics **in print**, (2006).

Cooper-White, J. J., J. E. Fagan, V. Tirtaatmadja, D. R. Lester and D. V. Boger, "Drop formation dynamics of constant low-viscosity, elastic fluids". Journal of Non-Newtonian Fluid Mechanics **106**, 29-59 (2002).

Doyle, P. S., E. S. G. Shaqfeh and A. P. Gast, "Dynamic simulation of freely draining flexible polymers in steady linear flows". Journal of Fluid Mechanics **334**, 251-291 (1997).

Dunlap, P. N. and L. G. Leal, "Dilute Polystyrene Solutions in Extensional Flows - Birefringence and Flow Modification". Journal of Non-Newtonian Fluid Mechanics **23**, 5-48 (1987).

Eggers, J., "Nonlinear dynamics and breakup of free-surface flows". Reviews of Modern Physics **69**, 865-929 (1997).

Entov, V. M. and E. J. Hinch, "Effect of a spectrum of relaxation times on the capillary thinning of a filament of elastic liquid". Journal of Non-Newtonian Fluid Mechanics **72**, 31-53 (1997).

Entov, V. M., V. I. Kordonskil and I. V. Prokhorov, "Rapid stretching of polymer solutions". Soviet Physics, Doklady **33**, 628-630 (1988).

Ferry, J. D., *Viscoelastic Properties of Polymers,* 1 ed., John Wiley & Sons, New York (1980).

Ghosh, I., G. H. McKinley, R. A. Brown and R. C. Armstrong, "Deficiencies of FENE dumbbell models in describing the rapid stretching of dilute polymer solutions". Journal of Rheology **45**, 721-758 (2001).

Graessley, W.W., "Polymer chain dimensions and the dependence of viscoelasic properties on the concentration, molecular weight and solvent power". Polymer **21**, 258-262 (1980).

Gupta, R. K., D. A. Nguyen and T. Sridhar, "Extensional viscosity of dilute polystyrene solutions: Effect of concentration and molecular weight". Physics of Fluids **12**, 1296-1318 (2000).

Harrison, G. M., J. Remmelgas and L. G. Leal, "The dynamics of ultradilute polymer solutions in transient flow: Comparison of dumbbell-based theory and experiment". Journal of Rheology **42**, 1039-1058 (1998).

Kalashnikov, V. N., "Shear-Rate Dependent Viscosity of Dilute Polymer-Solutions". Journal of Rheology **38**, 1385-1403 (1994).

Kolte, M. I. and P. Szabo, "Capillary thinning of polymeric filaments". Journal of Rheology **43**, 609-625 (1999).

Kulicke, W.-M. and C. Clasen, *Viscosimetry of Polymers and Polyelectrolytes,* Springer, Heidelberg (2004).

Larson, R. G., "The rheology of dilute solutions of flexible polymers: Progress and problems". Journal of Rheology **49**, 1-70 (2005).

Liang, R. F. and M. R. Mackley, "Rheological Characterization of the Time and Strain Dependence for Polyisobutylene Solutions". Journal of Non-Newtonian Fluid Mechanics **52**, 387-405 (1994).

Lindner, A., J. Vermant and D. Bonn, "How to obtain the elongational viscosity of dilute polymer solutions?" Physica A -Statistical Mechanics and Its Applications **319**, 125-133 (2003).

Mackay, M. E. and D. V. Boger, "An Explanation of the Rheological Properties of Boger Fluids". Journal of Non-Newtonian Fluid Mechanics **22**, 235-243 (1987).

Matta, J. E. and R. P. Tytus, "Liquid Stretching Using a Falling Cylinder". Journal of Non-Newtonian Fluid Mechanics **35**, 215-229 (1990).

McKinley, G. H., "Visco-Elasto-Capillary Thinning and Breakup of Complex Fluids", in: Binding, D. M. and K. Walters, (Eds.), *Annual Rheology Reviews*, (British Society of Rheology, Aberystwyth, 2005). pp. 1-48.

McKinley, G. H. and T. Sridhar, "Filament-stretching rheometry of complex fluids". Annual Review of Fluid Mechanics **34**, 375-415 (2002).

McKinley, G. H. and A. Tripathi, "How to extract the Newtonian viscosity from capillary breakup measurements in a filament rheometer". Journal of Rheology **44**, 653-670 (2000).

Nguyen, T. Q. and H. H. Kausch, *Flexible Polymer Chains in Elongational Flow: Theory & Experiment*, Springer-Verlag, Berlin (1999).

Öttinger, H. C., *Stochastic Processes in Polymeric Liquids,* Springer Verlag, Berlin (1996).

Papageorgiou, D. T., "On the Breakup of Viscous-Liquid Threads". Physics of Fluids **7**, 1529-1544 (1995).

Plog, J. P., W. M. Kulicke and C. Clasen, "Influence of the molar mass distribution on the elongational behaviour of polymer solutions in capillary breakup". Applied Rheology **15**, 28-37 (2005).

Rodd, L., T. Scott, J. Cooper-White and G. H. McKinely, "Cappillary Break-up Rheometry of Low-Viscosity Elastic Fluids". Applied Rheology **15**, 12-27 (2005).

Rubinstein, M. and R. H. Colby, *Polymer Physics,* Oxford University Press, New York (2003).

Slobozhanin, L. A. and J. M. Perales, "Stability of Liquid Bridges between Equal Disks in an Axial Gravity-Field". Physics of Fluids a-Fluid Dynamics **5**, 1305-1314 (1993).

Solomon, M. J. and S. J. Muller, "Study of mixed solvent quality in a polystyrene dioctyl phthalate polystyrene system". Journal of Polymer Science Part B-Polymer Physics **34**, 181-192 (1996).

Sridhar, T., V. Tirtaatmadja, D. A. Nguyen and R. K. Gupta, "Measurement of Extensional Viscosity of Polymer-Solutions". Journal of Non-Newtonian Fluid Mechanics **40**, 271-280 (1991).

Stelter, M. and G. Brenn, "Validation and application of a novel elongational device for polymer solutions". Journal of Rheology **44**, 595-616 (2000).

Stelter, M., G. Brenn, A. L. Yarin, R. P. Singh and F. Durst, "Investigation of the elongational behavior of polymer solutions by means of an elongational rheometer". Journal of Rheology **46**, 507-527 (2002).

Stoltz, C., J. J. dePablo and M. D. Graham, "Concentration dependence of shear and extensional rheology of polymer solutions: Brownian dynamics simulations". Journal of Rheology **50**, 137-167 (2006).

Tam, K. C. and C. Tiu, "Improved Correlation for Shear-Dependent Viscosity of Polyelectrolyte Solutions". Journal of Non-Newtonian Fluid Mechanics **46**, 275-288 (1993).

Tirtaatmadja, V., G. H. McKinley and J. J. Cooper-White, "Drop Formation and Breakup of Low Viscosity Elastic Fluids: Effects of Molecular Weight and Concentration". Physics of Fluids **in press**, (2006).

Yao, M. W., S. H. Spiegelberg and G. H. McKinley, "Dynamics of weakly strain-hardening fluids in filament stretching devices". Journal of Non-Newtonian Fluid Mechanics **89**, 1-43 (2000).

Appendix A

The following Figures 14 present the complete data set of capillary thinning experiments. Fig. 14b and 14c show the same data on two different time scales in order to capture the marked change in the relaxation time associated with changes in the polymer concentration c. from 5×10^4 ppm in DEP to 0.1 ppm in the viscous oligomer.

Figure 1 Comparison of the numerically calculated evolution in the filament diameter (open symbols) with experimental data from capillary thinning experiments (closed symbols) for a dilution series of the Boger fluid from sample E (M_w =8.3×10^6 g/mol) for different concentrations spanning five orders of magnitude. In addition the relaxation times τ_{exp}, determined from fitting the elasto-capillary thinning regime (Eq. 22) of the experiments, and τ_{num}, determined from fitting the numerical calculations (Eq. 17-21) to the experimental data, are given for selected concentrations.

Figure 2 Reduced diameter D/D_0 as a function of time t in capillary thinning experiments for several dilution series of narrowly distributed polystyrene samples. The samples are dissolved respectively in a) styrene oligomer (Boger fluids), determined from CCD camera video images of the thinning filament; b) styrene oligomer, determined with a laser micrometer; c) diethylphthalate (DEP), determined with a laser micrometer. In addition to the experimental data Fig. 2 b) also shows the theoretical critical concentrations $c^{\S}$ calculated from Eq. (41) that depicts the minimum concentration for an observable influence of polymer on the capillary thinning behaviour.

Figure 3 Relaxation time τ_0 as a function of the concentration c, determined by regression of the experimental data in the exponential decaying regime of Fig. 2 to Eq. (22). The dashed lines map the variation of relaxation time τ_0 with critical concentrations c^*. These values were determined by extrapolating the observed trends of relaxation times to the critical values determined from Eqs. (1) and (27).

Figure 4 a) Experimentally observed loss modulus G'' (upper curve) and storage modulus G' (lower curve) as a function of the angular frequency ω for a polystyrene dissolved in styrene oligomer (symbols) as well as the fits of Eqs. (2) and (3) to the experimental data (lines).
b) Storage moduli G' as a function of the angular frequency ω for different concentrations of polystyrene dissolved in styrene oligomer. In addition the fits of Eq. (2) to the experimental data are shown (lines). The lowest (dashed) line depicts the response of the pure oligomeric solvent which is weakly elastic with $\tau_s \approx 6.5\times10^{-4}$ s.
c) Reduced storage moduli $G'M_w/(cRT)$ as a function of the reduced frequency $\omega\tau_0$ for polystyrenes of different molar masses and concentrations. The longest relaxation times τ_0 were determined from fits of Eqs. (2) and (3) to the experimental data as shown in Fig. 4a.

Figure 5 Reduced relaxation time τ_0/τ_z as a function of the reduced concentration c/c*, determined from small amplitude oscillatory shear (SAOS) experiments and fits of the moduli to Eqs. (2) and (3) for polystyrene of different molar masses dissolved in styrene oligomer.

Figure 6 Reduced relaxation time τ_0/τ_z as a function of the reduced concentration c/c* for several dilution series of polystyrene Boger fluids determined from capillary break thinning experiments. In addition to the data obtained in this work, data points for the boger fluids SM1 (2·10^6 g/mol, ○), SM2 (6.5·10^6 g/mol, □) and SM3 (20·10^6 g/mol, ◊) are shown (taken from [7] and [20]). For comparison, also a mean square fit to the results from the SAOS experiments in Figure 5 is shown.

Figure 7 Stress distribution in capillary break-up-experiments. Shown are the driving capillary pressure and the stress distribution between the solvent and the polymer. Results were obtained from numerical calculations for three different concentrations c of polystyrene

in styrene oligomer for a constant Zimm relaxation time. The initial diameter of the filament was assumed as D_0 = 2.39 mm in accordance with experimental observations. The filament break-up times were a) $t_{br} = 11.41 \cdot \tau_0$, b) $t_{br} = 4.81 \cdot \tau_0$ c) $t_{br} = 2.82 \cdot \tau_0$. The right hand side shows the respective evolution of the chosen 8 modes of the configuration ($A_{zz,i}$-$A_{rr,i}$), with an increasing mode number i from top to bottom.

Figure 8 Numerical calculations of the diameter D/D_0 as a function of the reduced time t/τ_0 for a dilution series of polystyrene in styrene oligomer. Even though the longest relaxation time τ_0 is held *constant* for all calculations, only the calculations for the highest concentrations show a profile, in accordance with the indicated slope of $\exp(-t/3\tau_0)$ of Eq. (22).

Figure 9 Comparison of the numerically-calculated diameter evolution with experimental observations for a dilution series of a polystyrene Boger fluid with a molar mass $M_w = 2.8 \times 10^6$ g/mol. The initial diameters for the numerical calculations were taken from the experimental observations. In addition, the calculated evolution in stress distribution is given for each concentration. The critical concentration from Eq. (41) is $c^{\S}$ = 1.7 ppm.

Figure 10 Comparison of the numerically-calculated diameter evolution with experimental observations for a dilution series of a Boger fluid with a molar mass $M_w = 8.3 \times 10^6$ g/mol. The initial diameters for the numerical calculations were taken from the experimental observations. In addition, the calculated stress distribution is given for each concentration. The critical concentration from Eq. (41) is $c^{\S}$ = 0.36 ppm.

Figure 11 Reduced relaxation times τ_0/τ_z as a function of the reduced concentration c/c^*, obtained from best fits of the numerically calculated diameter evolution to the experiments presented in Figure 2 with τ_0 as an adjustable parameter (hollow symbols). For comparison, also the results from the SAOS experiments in Figure 7 are given (filled symbols). Also the range of critical concentrations $c^{\S}/c^*$ for the different molar masses is indicated by the rectangle.

Figure 12 Reduced relaxation times relaxation time τ_0/τ_z as a function of the reduced concentration $c[\eta]$ for dilution series of polystyrene in diethyl phthalate (DEP). In addition, the theoretical concentration dependence of the relaxation time according to Eq. (33) is shown. Also the range of critical concentrations $c^{\S}/c^*$ for the different molar masses is indicated by the rectangle.

Figure 13 Specific viscosity η_p/η_s as a function of the reduced concentration c/c^* for solutions of polystyrene in diethyl phthalate (DEP), determined with capillary viscometric measurements at lower concentrations, and cone-and-plate shear rheometry at higher concentrations The continuous line gives the best fit to the structure-property relationship of Eq. (32).

Figure 14 Reduced diameter D/D_0 as a function of time t in capillary thinning experiments for several dilution series of narrowly distributed polystyrene samples dissolved in: a) styrene oligomer, determined from CCD camera video images; b) styrene oligomer , determined with a laser micrometer. In addition to the experimental data Fig. 14 b) also shows the theoretical critical concentrations $c^{\S}$ calculated from Eq. (41) that depict the minimum

concentration for an observable influence of polymer on the capillary thinning behaviour; c) diethylphthalate (DEP), determined with a laser micrometer.

Table 1 Physical parameters of the polystyrene solutions in the near theta solvent styrene oligomer (Boger fluids).

Sample	M_w / (g/mol)	M_w/M_n	[η] / (cm^3/g)	L	η_s / (Pa s)	γ / (N/m)	ρ / (kg/m^3)	τ_z / s
A	1.80×10^6	1.02	103.8	122	33	0.0378	1026	0.74
B	2.84×10^6	1.13	122.1	157	51	0.0378	1026	2.16
C	5.67×10^6	1.09	156.8	229	45	0.0378	1026	4.84
D	6.00×10^6	1.22	160.0	237	33	0.0378	1026	3.83
E	8.27×10^6	1.13	178.8	280	45	0.0378	1026	7.95

Table 2 Physical parameters of the polystyrene solutions in the good solvent diethyl phthalate (DEP).

M_w / (g/mol)	M_w/M_n	[η] / (cm^3/g)	L	η_s / (Pa s)	γ / (N/m)	ρ / (kg/m^3)	τ_z / s
8.27×10^6	1.13	601	95.0	0.011	0.0375	1118	0.0107
5.67×10^6	1.09	464	81.1	0.011	0.0375	1118	0.0057
2.84×10^6	1.13	283	59.9	0.011	0.0375	1118	0.0017

Table 3 Critical concentrations for the polystyrene / styrene oligomer solutions (Boger fluids) determined from the intrinsic viscosity (Eq. (1)), the radius of gyration (Eq. (27)) and from Eq. (41).

M_w / (g/mol)	$c^*_{[\eta]}$ / (g/cm^3)	c^*_{Rg} / (g/cm^3)	$c^{\S}$ / (g/cm^3)
8.27×10^6	5.6×10^{-3}	7.0×10^{-3}	3.6×10^{-7}
6.00×10^6	6.2×10^{-3}	8.2×10^{-3}	5.6×10^{-7}
5.67×10^6	6.4×10^{-3}	8.4×10^{-3}	6.0×10^{-7}
2.84×10^6	7.0×10^{-3}	1.2×10^{-2}	1.7×10^{-6}
1.80×10^6	9.6×10^{-3}	1.5×10^{-2}	3.2×10^{-6}

Table 4 Critical concentrations for the polystyrene / diethyl phthalate (DEP) solutions, determined from the intrinsic viscosity (Eq. (1)) and from Eq. (41).

M_w / (g/mol)	$c^*_{[\eta]}$ / (g/cm^3)	$c^{\S}$ / (g/cm^3)
8.27×10^6	1.6×10^{-3}	8.4×10^{-7}
5.67×10^6	2.1×10^{-3}	1.5×10^{-6}
2.84×10^6	3.5×10^{-3}	4.5×10^{-6}

Table 5 Experimental and theoretical exponents m (Eq. (43)) and m_{theory} (Eq. (47)) for different solvent qualities

	ν	m_{theory}	m
PS Boger fluid	0.51	0.89	0.89
PEO in glycerol/water	0.55	0.54	0.65
PS in DEP	0.57	0.45	0.53

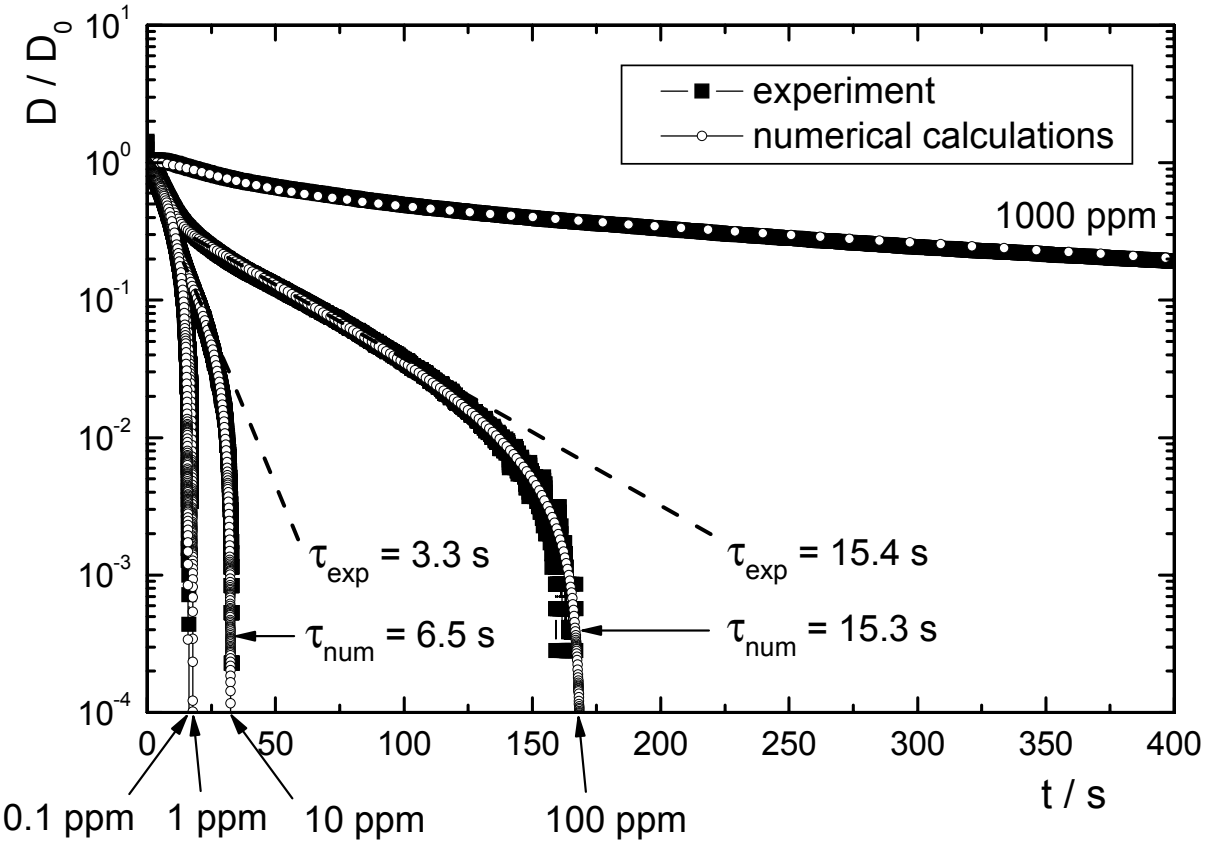
D / D0
experiment
numerical calculations
1000 ppm
τexp = 3.3 s
τexp = 15.4 s
τnum = 6.5 s
τnum = 15.3 s
0.1 ppm
1 ppm
10 ppm
100 ppm
t / s

Figure 1

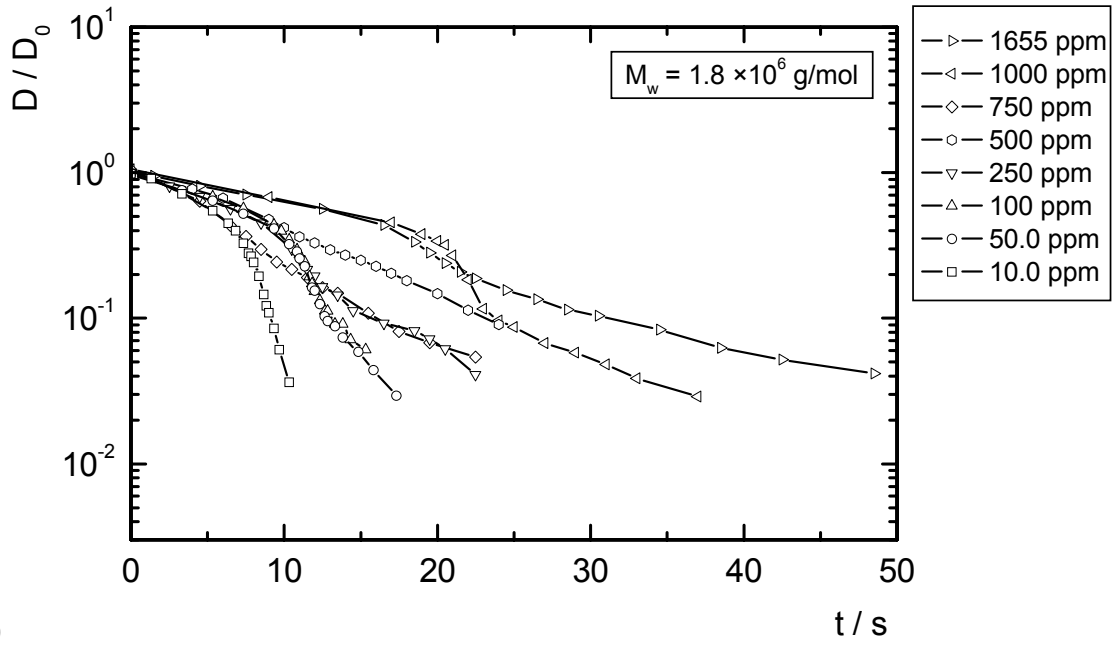
D / D0
Mw = 1.8 ×10^6 g/mol
1655 ppm
1000 ppm
750 ppm
500 ppm
250 ppm
100 ppm
50.0 ppm
10.0 ppm
t / s

a)

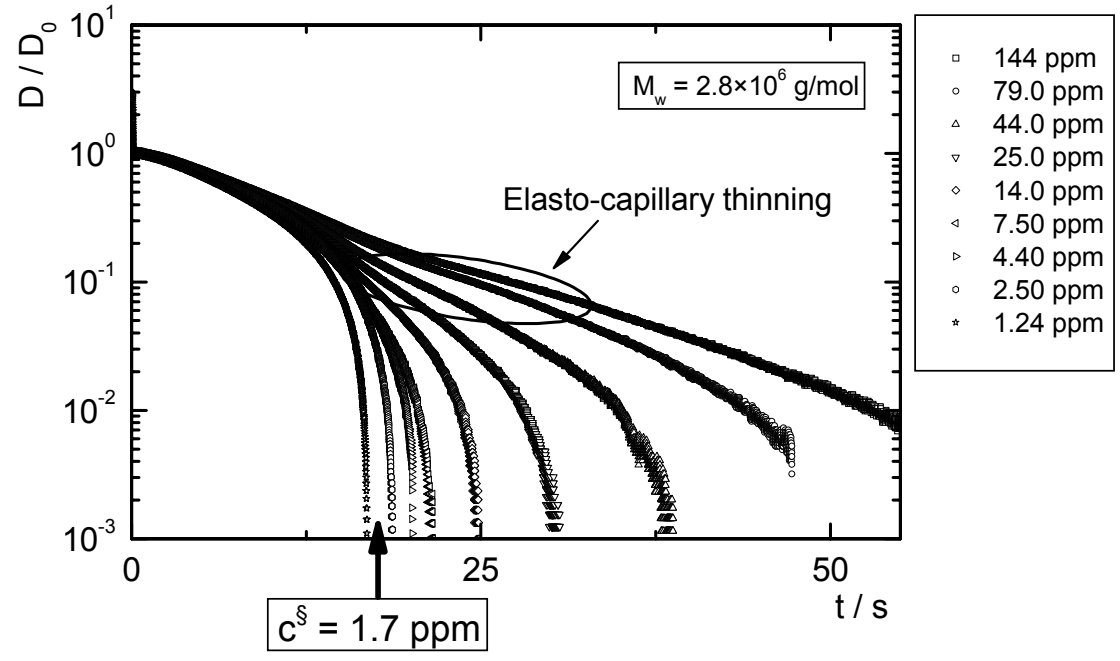
D / D0
Mw = 2.8×10^6 g/mol
144 ppm
79.0 ppm
44.0 ppm
25.0 ppm
14.0 ppm
7.50 ppm
4.40 ppm
2.50 ppm
1.24 ppm
Elasto-capillary thinning
c§ = 1.7 ppm
t / s

b)

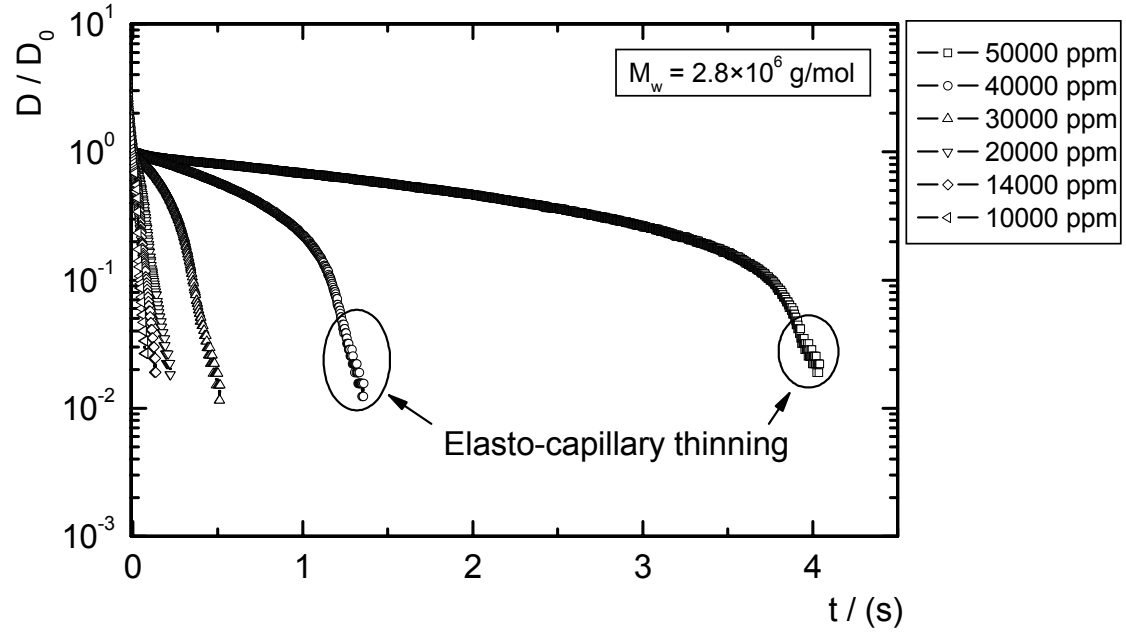
D / D0
Mw = 2.8×10^6 g/mol
50000 ppm
40000 ppm
30000 ppm
20000 ppm
14000 ppm
10000 ppm
Elasto-capillary thinning
t / (s)

c)

Figure 2

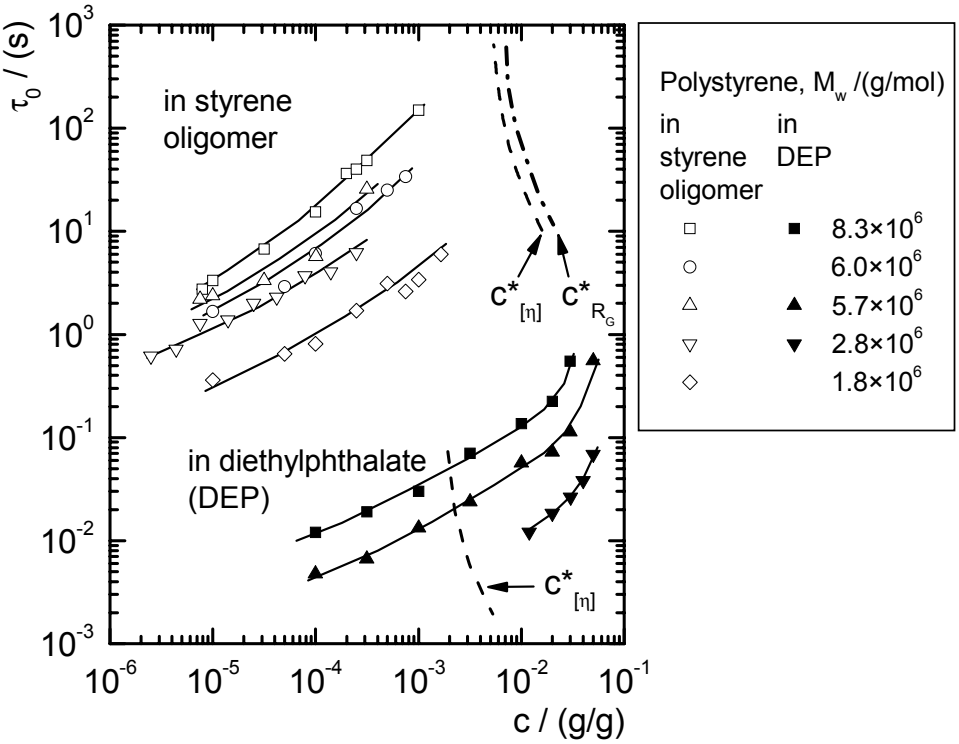
τ0 / (s)
in styrene oligomer
in diethylphthalate (DEP)
c*[η]
c*RG
c*[η]
c / (g/g)
Polystyrene, Mw /(g/mol)
in styrene oligomer
in DEP
8.3×10^6
6.0×10^6
5.7×10^6
2.8×10^6
1.8×10^6

Figure 3

a)

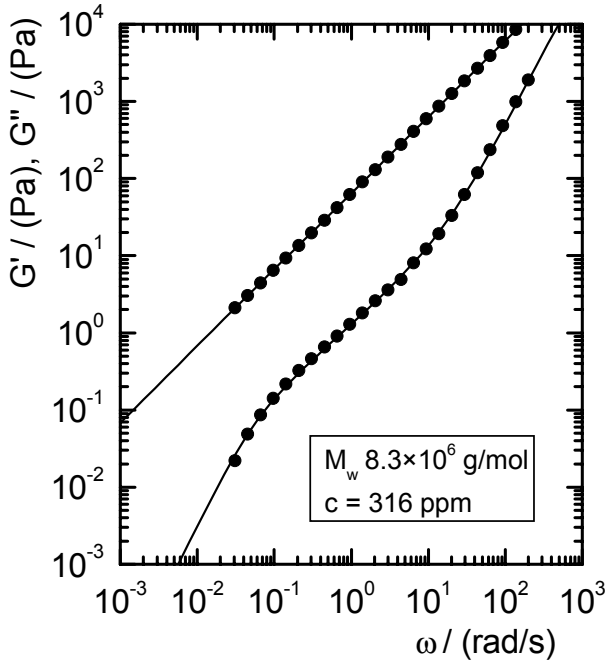
G' / (Pa), G'' / (Pa)
ω / (rad/s)
M_w 8.3×10^6 g/mol
c = 316 ppm

b)

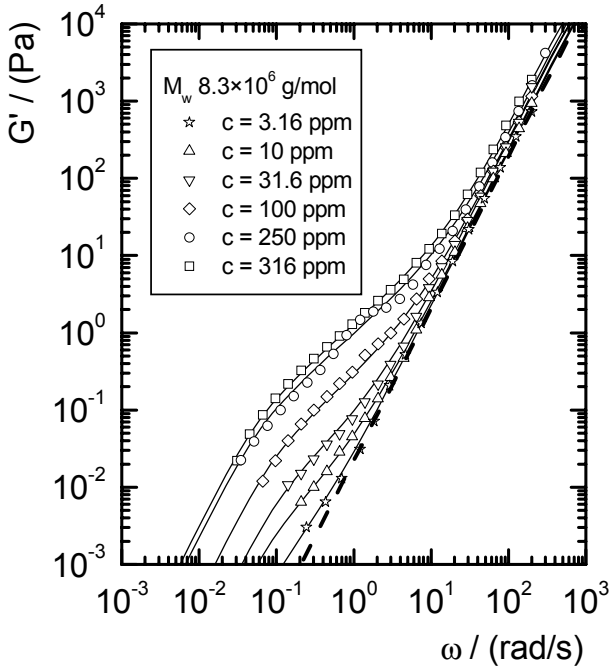
G' / (Pa)
ω / (rad/s)
M_w 8.3×10^6 g/mol
c = 3.16 ppm
c = 10 ppm
c = 31.6 ppm
c = 100 ppm
c = 250 ppm
c = 316 ppm

c)

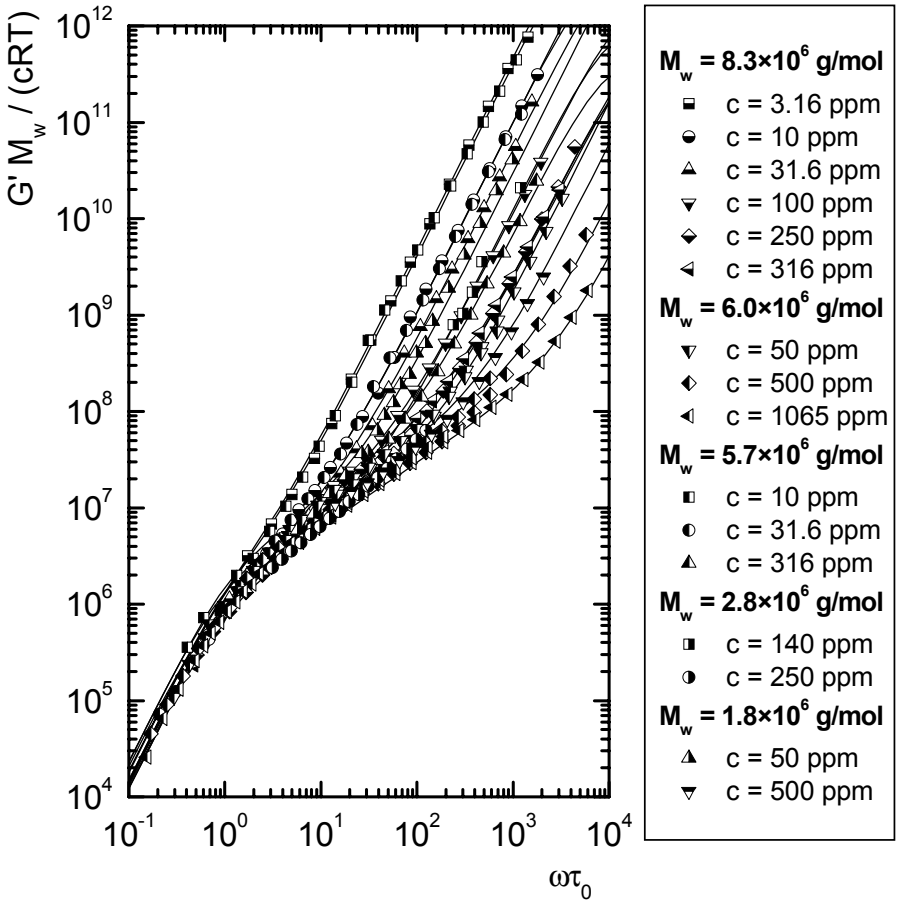
G' M_w / (cRT)
ωτ_0
M_w = 8.3×10^6 g/mol
c = 3.16 ppm
c = 10 ppm
c = 31.6 ppm
c = 100 ppm
c = 250 ppm
c = 316 ppm
M_w = 6.0×10^6 g/mol
c = 50 ppm
c = 500 ppm
c = 1065 ppm
M_w = 5.7×10^6 g/mol
c = 10 ppm
c = 31.6 ppm
c = 316 ppm
M_w = 2.8×10^6 g/mol
c = 140 ppm
c = 250 ppm
M_w = 1.8×10^6 g/mol
c = 50 ppm
c = 500 ppm

Figure 4

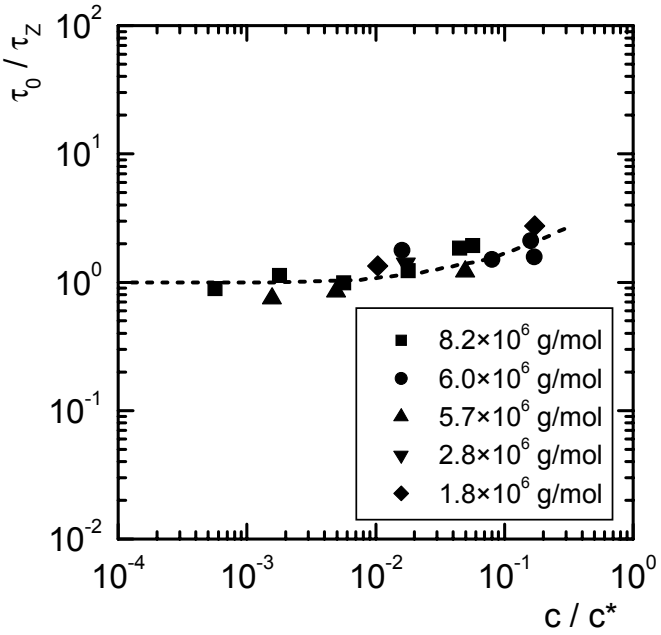
τ_0 / τ_Z
10^2
10^1
10^0
10^{-1}
10^{-2}
10^{-4}
10^{-3}
10^{-2}
10^{-1}
10^0
c / c*
8.2×10^6 g/mol
6.0×10^6 g/mol
5.7×10^6 g/mol
2.8×10^6 g/mol
1.8×10^6 g/mol

Figure 5

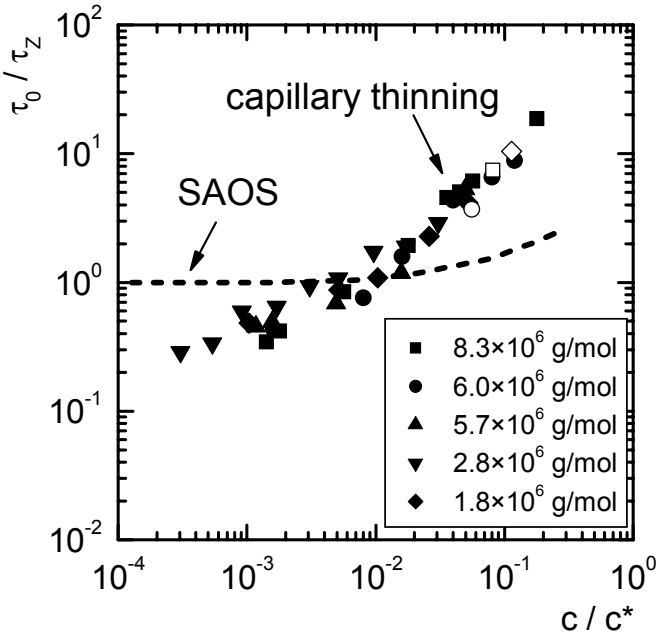
τ_0 / τ_Z
10^2
10^1
10^0
10^{-1}
10^{-2}
capillary thinning
SAOS
8.3×10^6 g/mol
6.0×10^6 g/mol
5.7×10^6 g/mol
2.8×10^6 g/mol
1.8×10^6 g/mol
10^{-4}
10^{-3}
10^{-2}
10^{-1}
10^0
c / c*

Figure 6

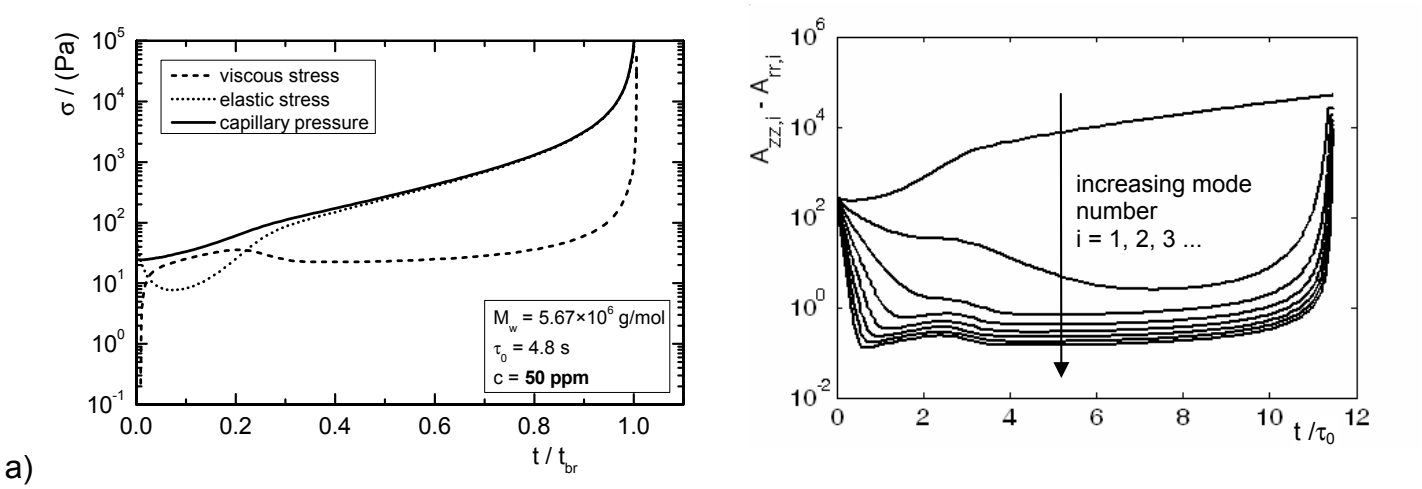
σ / (Pa)
viscous stress
elastic stress
capillary pressure
M_w = 5.67×10^6 g/mol
τ_0 = 4.8 s
c = 50 ppm
t / t_{br}
$A_{zz,i}$ - $A_{rr,i}$
increasing mode number
i = 1, 2, 3 ...
t /τ_0

a)

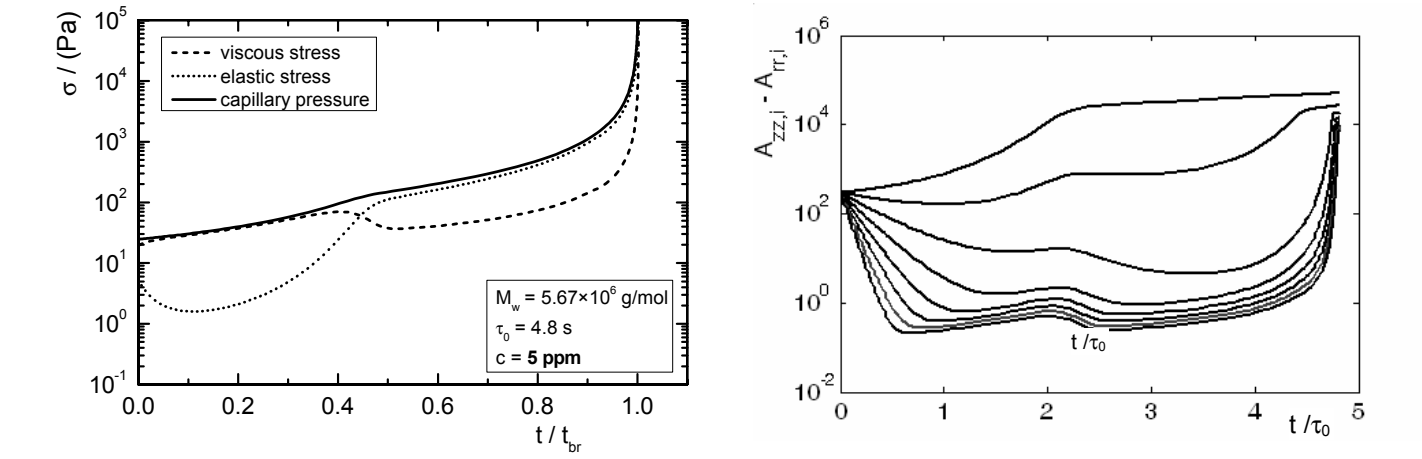
σ / (Pa)
viscous stress
elastic stress
capillary pressure
M_w = 5.67×10^6 g/mol
τ_0 = 4.8 s
c = 5 ppm
t / t_{br}
$A_{zz,i}$ - $A_{rr,i}$
t /τ_0

b)

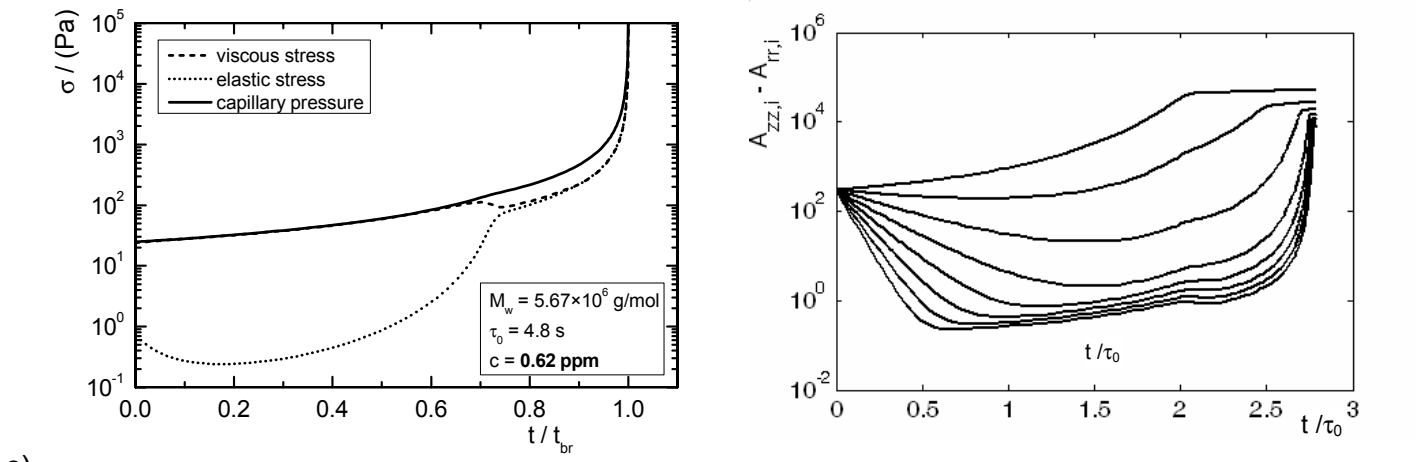
σ / (Pa)
viscous stress
elastic stress
capillary pressure
M_w = 5.67×10^6 g/mol
τ_0 = 4.8 s
c = 0.62 ppm
t / t_{br}
$A_{zz,i}$ - $A_{rr,i}$
t /τ_0

c)

Figure 7

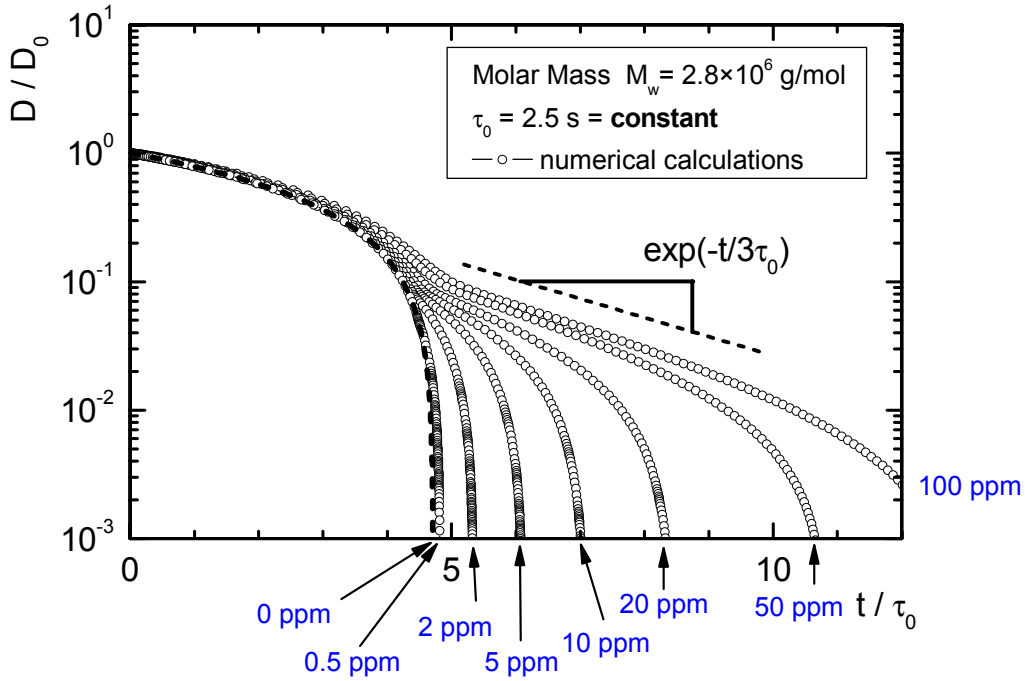
D / D0
Molar Mass Mw = 2.8×10^6 g/mol
τ0 = 2.5 s = constant
numerical calculations
exp(-t/3τ0)
100 ppm
0 ppm
0.5 ppm
2 ppm
5 ppm
10 ppm
20 ppm
50 ppm
t / τ0

Figure 8

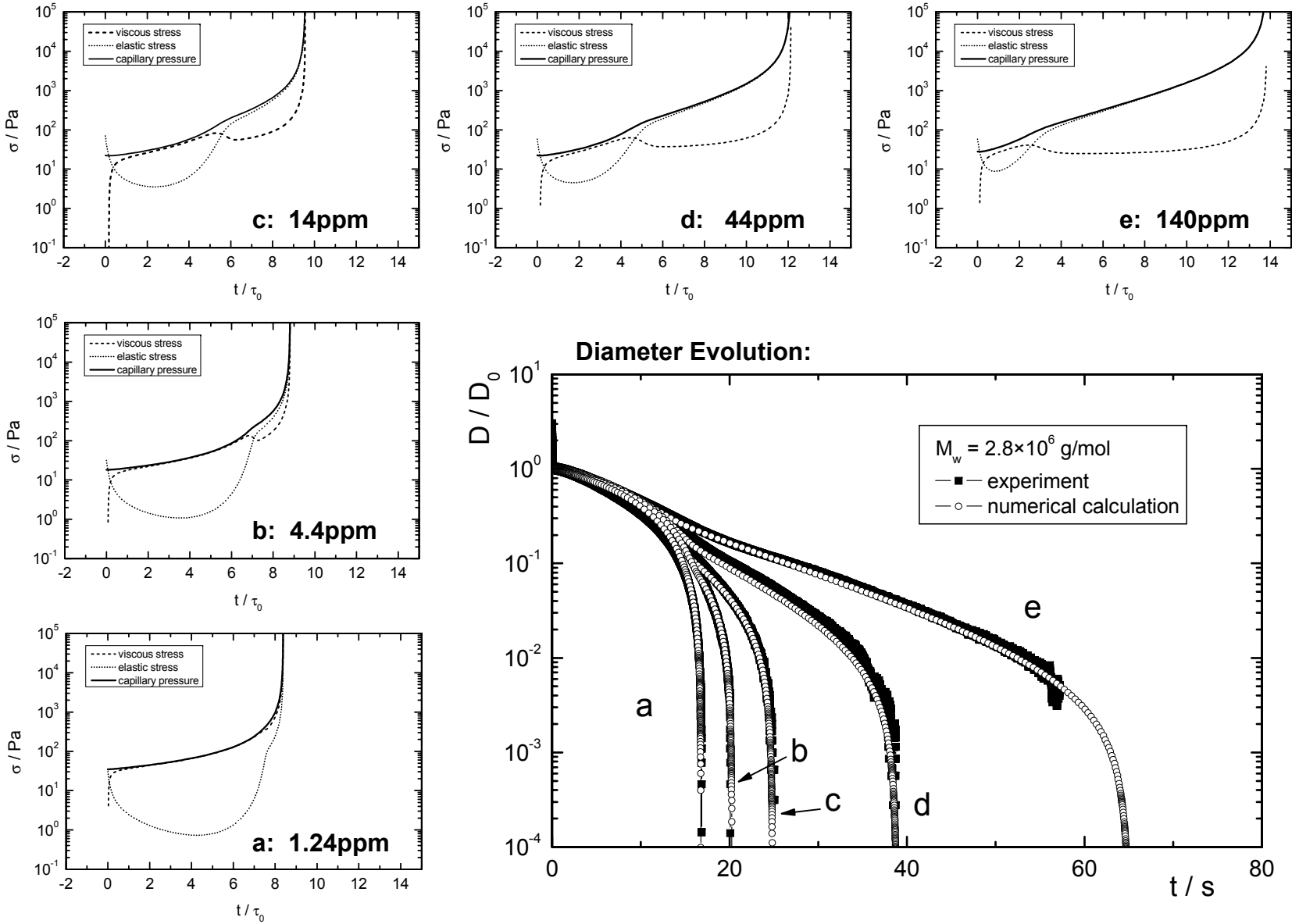
viscous stress
elastic stress
capillary pressure
σ / Pa
t / τ0
c: 14ppm
d: 44ppm
e: 140ppm
b: 4.4ppm
a: 1.24ppm
Diameter Evolution:
D / D0
Mw = 2.8×10^6 g/mol
experiment
numerical calculation
a
b
c
d
e
t / s

Figure 9

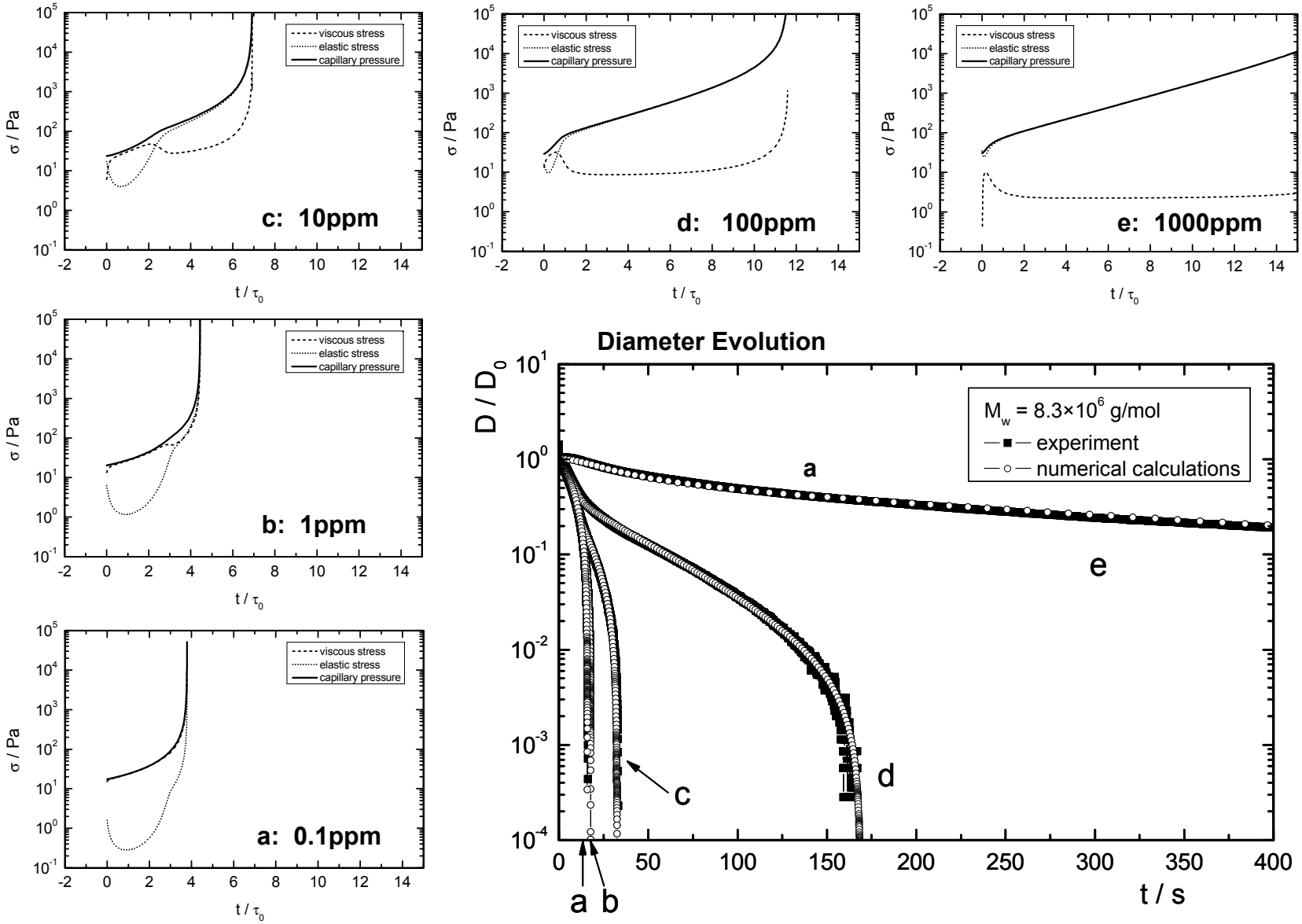
viscous stress
elastic stress
capillary pressure
σ / Pa
t / τ0
c: 10ppm
d: 100ppm
e: 1000ppm
b: 1ppm
a: 0.1ppm
Diameter Evolution
D / D0
Mw = 8.3×10^6 g/mol
experiment
numerical calculations
a
b
c
d
e
t / s

Figure 10

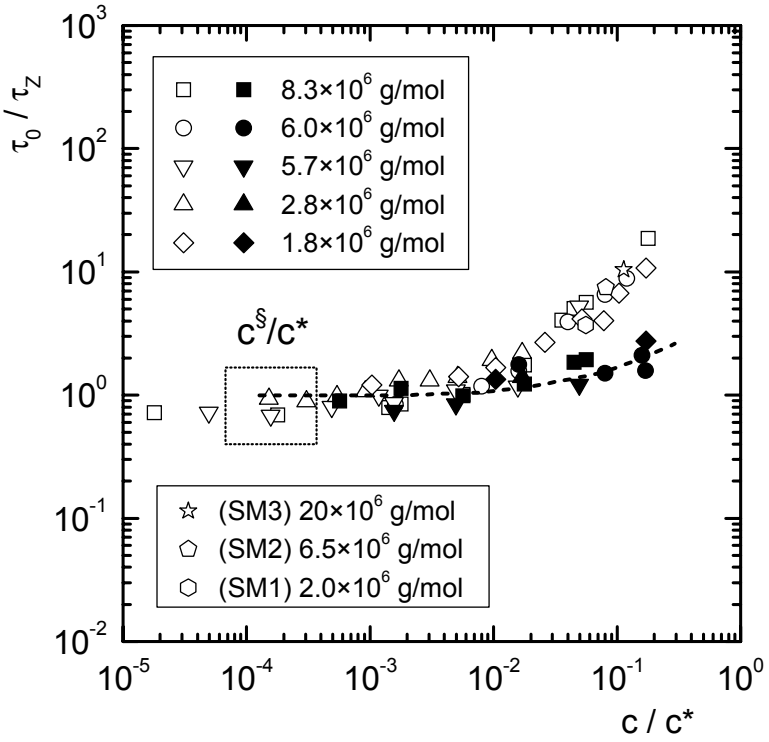
10^3
10^2
10^1
10^0
10^{-1}
10^{-2}
τ_0 / τ_Z
8.3×10^6 g/mol
6.0×10^6 g/mol
5.7×10^6 g/mol
2.8×10^6 g/mol
1.8×10^6 g/mol
c§/c*
(SM3) 20×10^6 g/mol
(SM2) 6.5×10^6 g/mol
(SM1) 2.0×10^6 g/mol
10^{-5}
10^{-4}
10^{-3}
10^{-2}
10^{-1}
10^0
c / c*

Figure 11

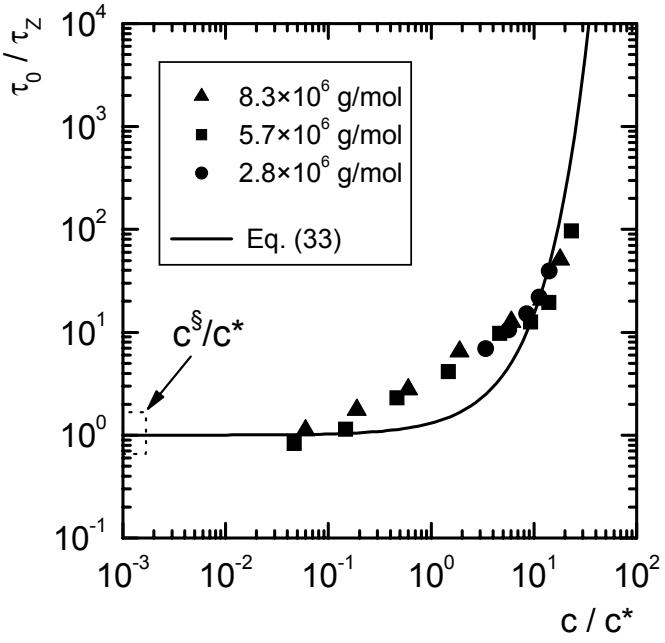
τ0 / τZ
10^4
10^3
10^2
10^1
10^0
10^-1
8.3×10^6 g/mol
5.7×10^6 g/mol
2.8×10^6 g/mol
Eq. (33)
c§/c*
10^-3
10^-2
10^-1
10^0
10^1
10^2
c / c*

Figure 12

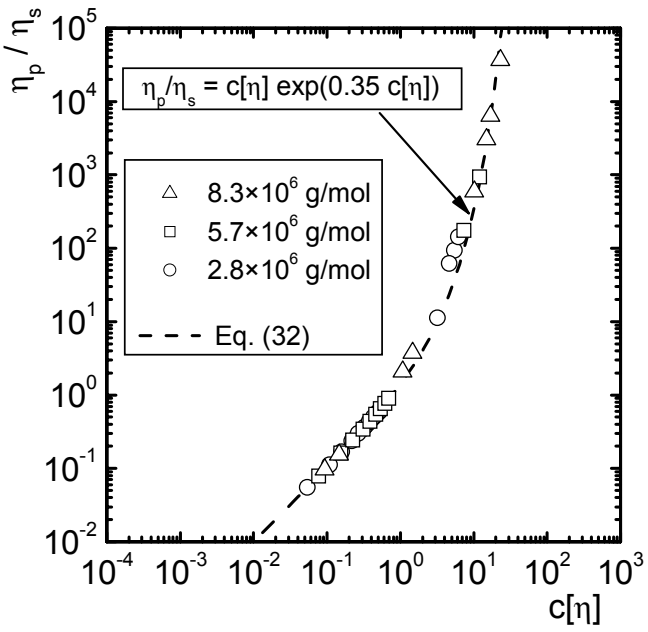
η_p / η_s
η_p/η_s = c[η] exp(0.35 c[η])
8.3×10^6 g/mol
5.7×10^6 g/mol
2.8×10^6 g/mol
Eq. (32)
c[η]

Figure 13

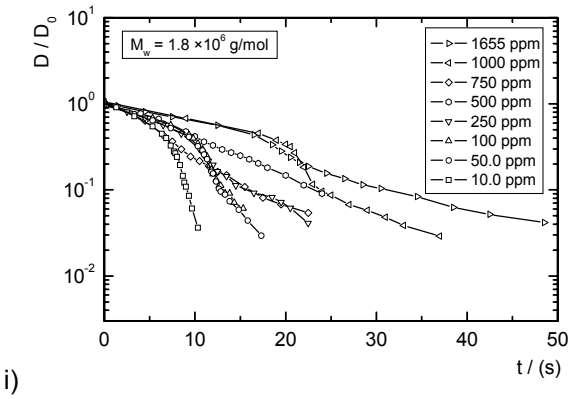

i)

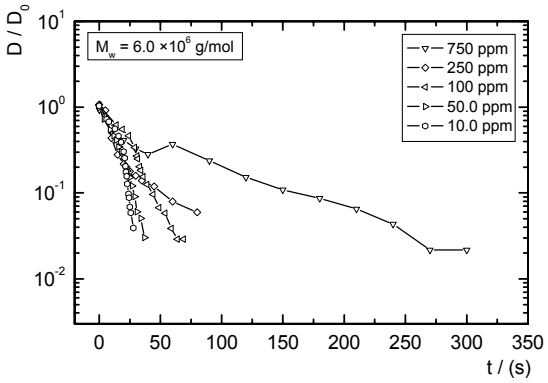

ii)

Figure 14a

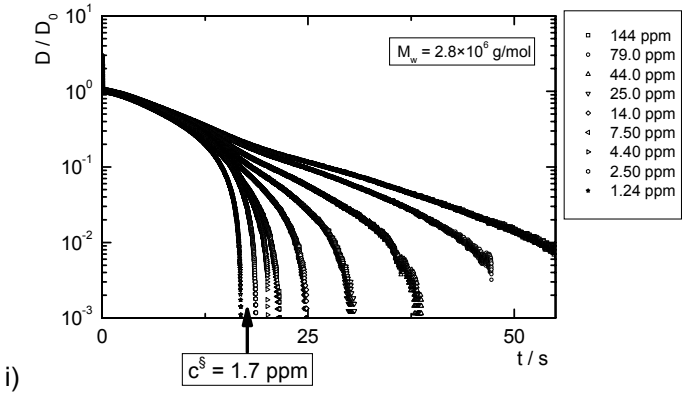

i)

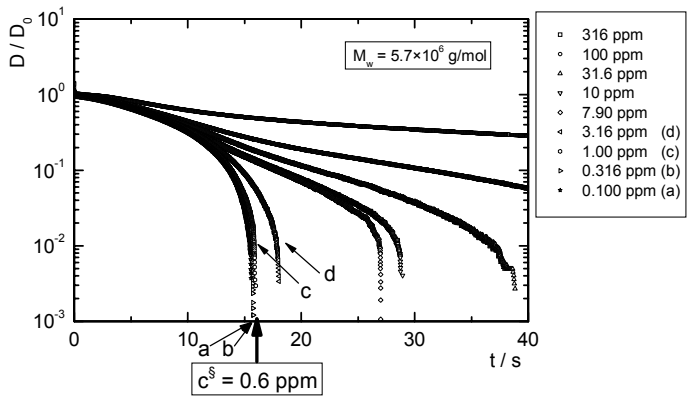

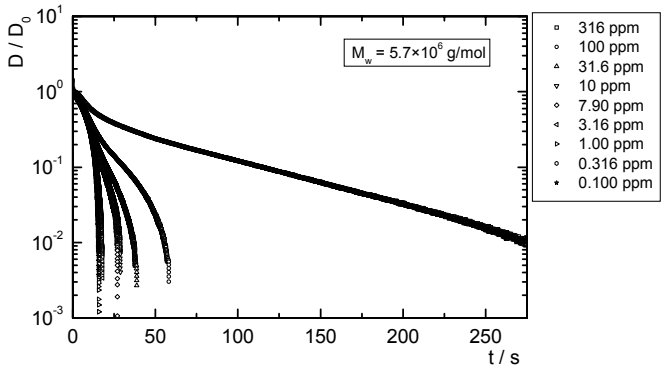

ii)

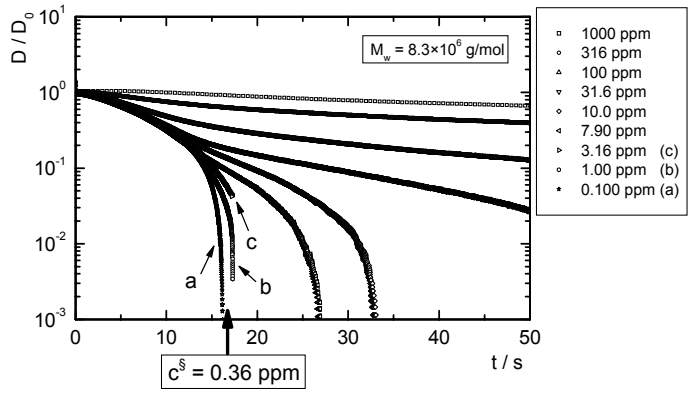

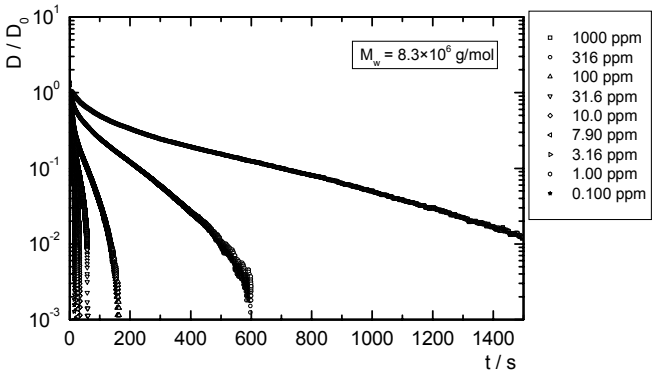

iii)

Figure 14b

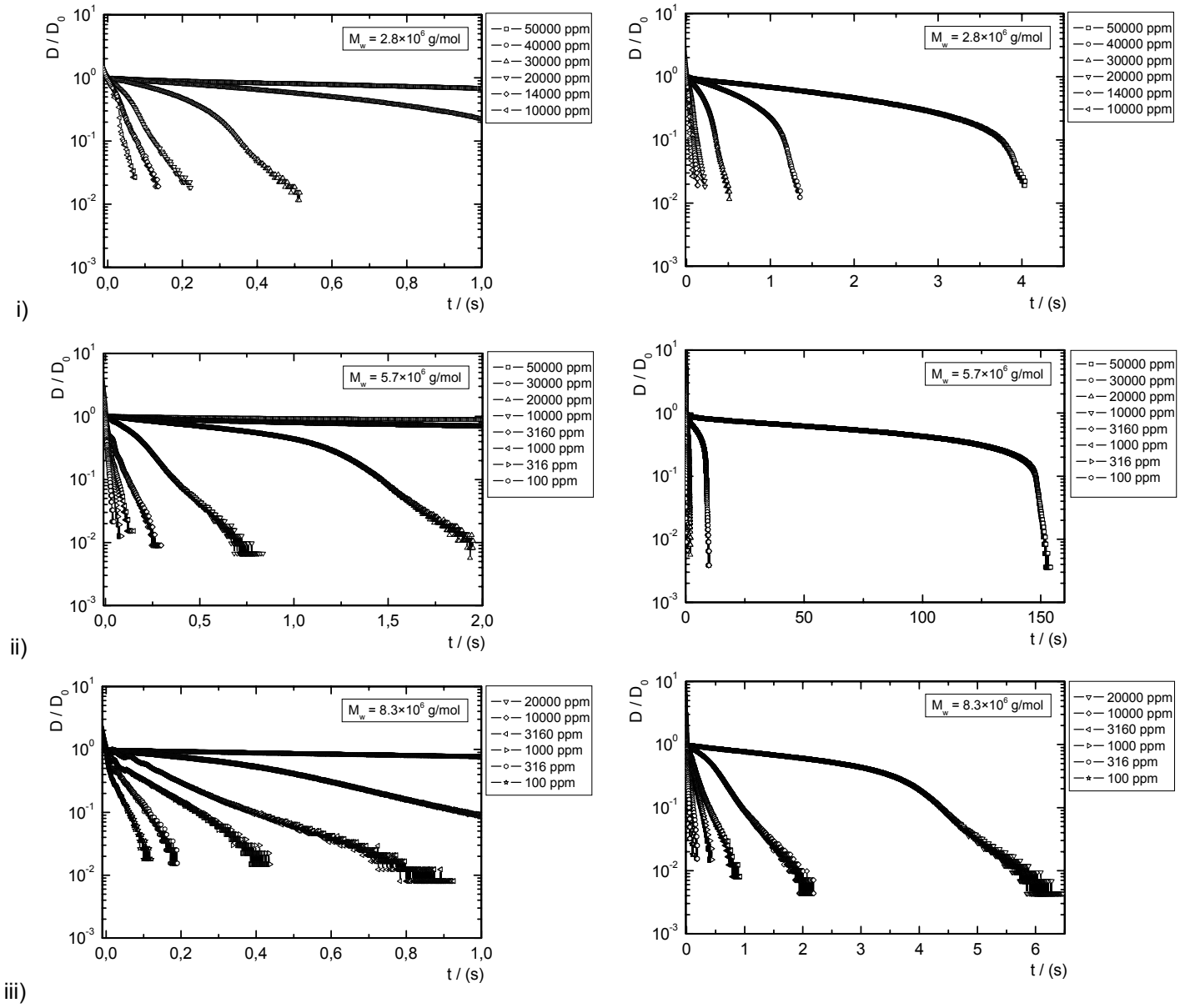
i)
D / D0
M_w = 2.8×10^6 g/mol
50000 ppm
40000 ppm
30000 ppm
20000 ppm
14000 ppm
10000 ppm
t / (s)
ii)
M_w = 5.7×10^6 g/mol
50000 ppm
30000 ppm
20000 ppm
10000 ppm
3160 ppm
1000 ppm
316 ppm
100 ppm
iii)
M_w = 8.3×10^6 g/mol
20000 ppm
10000 ppm
3160 ppm
1000 ppm
316 ppm
100 ppm

Figure 14c